

# THE REST FRAME OPTICAL SPECTRA OF LYMAN BREAK GALAXIES: STAR FORMATION, EXTINCTION, ABUNDANCES, AND KINEMATICS<sup>1</sup>

MAX PETTINI

Institute of Astronomy, Madingley Road, Cambridge, CB3 0HA, UK

ALICE E. SHAPLEY AND CHARLES C. STEIDEL<sup>2</sup>

Palomar Observatory, California Institute of Technology, MS 105-24, Pasadena, CA 91125

JEAN-GABRIEL CUBY

European Southern Observatory, Alonso de Cordova 3107, Santiago, Chile

MARK DICKINSON

Space Telescope Science Institute, 3700 San Martin Drive, Baltimore, MD 21218

ALAN F.M. MOORWOOD

European Southern Observatory, Karl-Schwarzschild-Str. 2, D-85748 Garching, Germany

KURT L. ADELBERGER<sup>3</sup>

Harvard-Smithsonian Center for Astrophysics, 60 Garden Street, Cambridge, MA 02138

MAURO GIAVALISCO

Space Telescope Science Institute, 3700 San Martin Drive, Baltimore, MD 21218

---

<sup>1</sup>Based on data obtained at the European Southern Observatory on Paranal, Chile, and at the W.M. Keck Observatory on Mauna Kea, Hawaii. The W.M. Keck Observatory is operated as a scientific partnership among the California Institute of Technology, the University of California, and NASA, and was made possible by the generous financial support of the W.M. Keck Foundation.

<sup>2</sup>Packard Fellow.

<sup>3</sup>Harvard Junior Fellow.

## ABSTRACT

We present the first results of a spectroscopic survey of Lyman break galaxies (LBGs) in the near-infrared aimed at detecting the emission lines of [O II], [O III], and  $H\beta$  from the H II regions of normal star forming galaxies at  $z \simeq 3$ . From observations of 15 objects with the Keck and VLT telescopes, augmented with data from the literature for an additional four, we reach the following main conclusions. The rest-frame optical properties of LBGs at the bright end of the luminosity function are remarkably uniform; their spectra are dominated by emission lines, [O III] is always stronger than  $H\beta$  and [O II], and projected velocity dispersions are between 50 and  $115 \text{ km s}^{-1}$ . Contrary to expectations, the star formation rates deduced from the  $H\beta$  luminosity are on average no larger than those implied by the stellar continuum at  $1500\text{\AA}$ ; presumably any differential extinction between rest-frame optical and UV wavelengths is small compared with the relative uncertainties in the calibrations of these two star formation tracers. For the galaxies in our sample, the abundance of oxygen can only be determined to within one order of magnitude without recourse to other emission lines ([N II] and  $H\alpha$ ) which are generally not available. Even so, it seems well established that LBGs are the most metal-enriched structures at  $z \simeq 3$ , apart from QSOs, with abundances greater than about 1/10 solar and generally higher than those of damped Lyman  $\alpha$  systems at the same epoch. They are also significantly overluminous for their metallicities; this is probably an indication that their mass-to-light ratios are low compared with present-day galaxies. At face value the measured velocity dispersions imply virial masses of about  $10^{10} M_{\odot}$  within half-light radii of 2.5 kpc. The corresponding mass-to-light ratios,  $M/L \approx 0.15$  in solar units, are indicative of stellar populations with ages between  $10^8$  and  $10^9$  years, consistent with the optical-IR spectral energy distributions. However, we are unable to establish conclusively if the widths of the emission lines do reflect the motions of the H II regions within the gravitational potential of the galaxies, even though in two cases we see hints of rotation curves. All 19 LBGs observed show evidence for galactic-scale superwinds; such outflows have important consequences for regulating star formation, distributing metals over large volumes, and allowing Lyman continuum photons to escape and ionize the intergalactic medium.

*Subject headings:* cosmology:observations — galaxies:abundances — galaxies:evolution — galaxies:starburst — infrared:galaxies

## 1. Introduction

Our current knowledge of the normal galaxy population at high redshift relies heavily on observations in the rest frame ultraviolet (UV) region, where we see the integrated light of OB stars and the strongest spectral features are interstellar absorption lines (e.g. Steidel et al. 1996, 1999; Lowenthal et al. 1996; Pettini et al. 2000; Steidel, Pettini, & Adelberger 2001). The situation is quite different at low redshift where the UV spectra of star forming galaxies have become accessible only relatively recently, requiring observations from space with the *Hubble Space Telescope* (*HST*; see Leitherer 2000 for a recent overview). For the last fifty years local galaxies with active star formation have been studied first and foremost at optical wavelengths through the rich emission line spectrum produced by their H II regions.

There is therefore a strong incentive to obtain such spectra for galaxies at  $z \simeq 3$  where the samples of UV-selected objects now number nearly one thousand. Apart from the surprises often associated with opening a new wavelength window, there are several obvious scientific motivations. The luminosity of the Balmer lines, primarily H $\alpha$  and H $\beta$ , gives a measure of the star formation rate which is directly comparable to the values deduced in local surveys. Furthermore, since the optical emission lines and the far-UV continuum do not respond to dust extinction to the same degree, the relative luminosity of a galaxy in these two tracers of star formation could in principle be used as a reddening indicator. When integrated over an entire galaxy, the widths of the nebular lines should reflect the velocity dispersion of the H II regions within the overall gravitational potential so that a kinematical mass may be deduced. This is not possible in the UV, because the interstellar absorption lines are sensitive to small amounts of gas accelerated to high velocities by energetic events such as supernova explosions and bulk outflows, while the stellar absorption lines from OB stars are intrinsically broad. Finally, there are well established chemical abundance diagnostics based on the relative strengths of nebular emission lines, primarily [O II], [O III] and H $\beta$ . Abundance measurements are much more difficult in the UV where the more easily observed interstellar lines are generally saturated so that their equivalent widths depend mostly on the velocity dispersion of the gas and only to a lesser extent on the column density of the absorbing ions.

At  $z \simeq 3$  the most prominent lines from H II regions are redshifted into the near-infrared (IR) where observations are more challenging than at optical wavelengths. Not only does atmospheric absorption by water vapour limit observations to specific wavelength bands, but even in these the night sky glows brightly in numerous OH emission lines which vary in intensity over timescales of minutes. However, with a large sample of galaxies such as that produced by the Lyman break technique (Steidel 2000) it is possible to isolate redshifts which place the transitions of interest in gaps between the OH sky lines; here the background is sufficiently dark for faint extragalactic work to become possible. In Pettini et al. (1998) we proved the feasibility of this approach with *K*-band observations of five Lyman break galaxies (LBGs) using the CGS4 spectrograph on the 3.8 m United Kingdom Infrared Telescope (UKIRT). Although successful, these initial attempts showed that galaxies at  $z \simeq 3$  are generally too faint to be studied in large numbers with 4-m

class telescopes. The five galaxies targeted by Pettini et al. are among the brightest LBGs known and still required essentially one night of integration per object with CGS4. On the other hand, the recent commissioning of near-IR, high resolution spectrographs on the Keck II and VLT1 telescopes now makes it possible to extend this work to a larger and more representative sample of high redshift galaxies. We have begun such a program of near-IR spectroscopy and present here our results for 15 Lyman break galaxies. Preliminary reports have been published in conference proceedings (Pettini 2000; Cuby et al. 2000) and similar observations of individual galaxies have also been obtained by Teplitz et al. (2000a,b) and Kobulnicky & Koo (2000).

This paper is arranged as follows. In §2 we summarize details of the observation and data reduction procedures. Individual objects with features of special interest are discussed in §3. In §4 we present our measurements of  $H\beta$  luminosity, derive star formation rates, and compare them with the values deduced from the UV continuum. §5 deals with the abundance of Oxygen derived from the strong line ratios, while in §6 we analyze the kinematics of the galaxies observed. The most important results of this work are reviewed in §7. Unless otherwise stated, we adopt a  $\Omega_M = 0.3$ ,  $\Omega_\Lambda = 0.7$ ,  $H_0 = 70 \text{ km s}^{-1} \text{ Mpc}^{-1}$  cosmology throughout the paper.

## 2. Observations

Details of the Lyman break galaxies observed are collected in Table 1. The optical redshifts listed in columns (4) and (5) were measured from  $12.5 \text{ \AA}$  resolution spectra obtained with the Low Resolution Imaging Spectrograph on the Keck telescopes. The optical photometry is from our  $U_n$ ,  $G$ ,  $\mathcal{R}$  deep imaging at the prime foci of the Palomar 5-m, La Palma 4.2-m, and Kitt Peak 4-m telescopes, while the  $(\mathcal{R} - K_{AB})$  colors listed in column (7) are from the survey by Shapley et al. (in preparation) conducted with the Keck Near-Infrared Camera (NIRC). Objects were selected from a variety of fields, some including high redshift QSOs and radio galaxies, others being blank regions of sky already targeted by other deep surveys such as the Hawaii deep field SSA22, the Caltech Deep Field, and the Groth-Westphal strip. Coordinates of all the objects observed are given in columns (2) and (3) of Table 1.

The primary selection criterion in compiling the sample in Table 1 was redshift; as explained above we aimed to minimize the chance of interference from bright sky lines. We also limited ourselves to galaxies brighter than  $\mathcal{R} \simeq 24.2$  which at  $z \simeq 3$  corresponds to  $\sim 1.3 L^*$  in the rest frame ultraviolet (Steidel et al. 1999); thus the galaxies observed are drawn from the brightest 10% of the full sample of more than 800 spectroscopically confirmed LBGs with  $\mathcal{R} \leq 25.5$  (Steidel 2000). We further attempted to span a range of  $(G - \mathcal{R})$  colors so as to sample objects with different UV continuum slopes, presumably reflecting different degrees of dust extinction. None of the galaxies show evidence for nuclear activity in their rest frame UV spectra. Most of the observations were targeted at  $H\beta$  ( $\lambda 4861.32$ ) and the [O III] doublet ( $\lambda\lambda 4958.91, 5006.84$ ) in the  $K$ -band; in a few additional cases we also searched for the corresponding [O II] ( $\lambda\lambda 3726.05, 3728.80$ ) in the  $H$ -band.

## 2.1. Data Acquisition

The data were secured during four observing runs in 1999 and 2000 using the NIRSPEC and ISAAC spectrographs on the Keck II and VLT1 telescopes respectively (see last column of Table 1).

A detailed description of NIRSPEC is given by McLean et al. (1998). It uses a  $1024 \times 1024$   $27\mu\text{m}$  pixel (ALADDIN2) InSb detector; in the medium dispersion mode employed for the present observations each detector pixel corresponds to 0.143 arcsec in the spatial direction and the dispersion in the spectral direction is  $4.2 \text{ \AA}/\text{pixel}$ . In the September 1999 observing run we used an entrance slit 0.57 arcsec wide which gives a spectral resolution of  $11.6 \text{ \AA}$  FWHM (resolving power  $R \simeq 1750$  at  $2.05 \mu\text{m}$ ) sampled with 2.8 wavelength bins (measured from the widths of sky emission lines in the reduced spectra). In April 2000 we changed to the wider 0.76 arcsec entrance slit, giving a resolution of  $13.6 \text{ \AA}$  FWHM (resolving power  $R \simeq 1500$ ) sampled with 3.2 bins. The galaxies to be observed were placed in the slit by offsetting from a nearby bright star. This manoeuvre was 'blind' in the sense that normally the galaxy and the offset star were separated by more than the 42 arcsec length of the NIRSPEC slit; however, on no occasion did we fail to acquire the target. Individual exposure times were 900 s; the detector was read out in multiple read mode (16 reads at the start and the end of each integration) to reduce noise. After each exposure the offsetting procedure was repeated and the target reacquired at a different position on the slit, typically 5 arcsec from the previous one. Conditions were mostly photometric during both Keck runs and the typical seeing in the  $K$ -band was 0.5–0.6 arcsec FWHM.

The short wavelength channel of ISAAC (Moorwood et al. 1999) uses a  $1024 \times 1024$   $18.5\mu\text{m}$  pixel Rockwell array; the projected pixel scale along the slit is very similar to that of NIRSPEC, 0.146 arcsec/pixel. The spectral dispersion, however, is 2.3 times higher at  $1.24 \text{ \AA}/\text{pixel}$ ; with the 1 arcsec wide slit we used, the resolution is  $7.4 \text{ \AA}$  FWHM ( $R \simeq 2750$ ) sampled with six wavelength bins. Acquisition was also achieved via nearby bright stars; in this case however the 120 arcsec long ISAAC slit allowed us to have both offset star and target galaxy on the slit at the same time (having rotated the slit to the required position angle on the sky). The bright star spectrum is a useful reference for verifying the accuracy of the offsetting procedure, and monitoring seeing and sky transparency fluctuations. Our two VLT runs in September and November 1999 were mostly photometric and the seeing varied between 0.5 and 0.9 arcsec. The ISAAC observations were performed in beam-switching mode with the object moved between two positions on the slit separated by 10 arcsec. After an A-B-B-A series of  $4 \times 900$  s long exposures, the object was reacquired at a different position along the slit, and the four-exposure sequence repeated.

## 2.2. Data Reduction

Examples of NIRSPEC and ISAAC spectra of Lyman break galaxies in the  $K$ -band are reproduced in Figures 1 and 2 respectively, while Figure 3 shows detections of [O II]  $\lambda 3727$  in the

*H*-band. In Figure 2 the ISAAC spectra have been rebinned to twice the original pixel size, so that the spectral resolution is sampled with three wavelength bins in these plots.

The two-dimensional data frames were reduced using a series of IRAF scripts, following the same basic steps for NIRSPEC and ISAAC spectra. After flat-fielding (by reference to the spectrum of a quartz halogen lamp), correcting for defective pixels (flagged from the analysis of the noise in flat-field and dark current frames), and rotating the images (so as to align the spectrum approximately along the columns of the detector), we applied a geometric transformation to correct for the spatial distortion and spectral curvature introduced by the spectrograph optics. The two-dimensional map used in this transformation was obtained by stepping a bright star in regular intervals along the slit and determining the star trace as a function of slit position. The rectified 2-D images were wavelength calibrated on a vacuum scale with the aid of the atlas of OH sky emission lines by Rousselot et al. (2000). The next steps in the reduction differed slightly between NIRSPEC and ISAAC spectra.

With NIRSPEC we moved the object along the slit every 900 s exposure. Consequently, we used the exposures immediately preceding and following a given image to construct a sky frame which was then subtracted in 2-D from each image, after appropriate line-by-line scaling. A further background correction was applied to each sky-subtracted image (by fitting a polynomial in the spatial direction at each wavelength bin) to remove the residuals at the wavelengths of the strongest sky lines. The individual frames so processed were then registered and co-added (with a rejection algorithm to exclude cosmic rays and other invalid pixels) to produce a fully reduced, two-dimensional spectrum of each galaxy observed. The final step in the reduction involved extracting one-dimensional spectra by summing the signal along the slit; we applied both weighted and unweighted extractions, but found the two methods to give very similar results. The IRAF scripts used in the manipulation of the data frames also generate at each step a corresponding 2-D frame of the statistical  $1\sigma$  error appropriate to each pixel; in the last step this is used to produce the one-dimensional error spectrum applicable to the extracted galaxy spectrum.

Since the ISAAC observations were obtained in beam-switching mode, sky subtraction was achieved by adding separately the pair of frames with the object at position A and the pair with the object at position B. Two difference images were then produced from these pairs: A–B and B–A. After registering one difference image onto the other by the known A-B telescope offset, the two were added together; this produces a characteristic 2-D image with a positive galaxy spectrum flanked by two negative spectra (separated from the positive spectrum by the A-B spatial offset). Our observations usually consisted of a series of three or five such A-B-B-A patterns (at different positions along the slit); these were combined and extracted in the same way as the NIRSPEC spectra.

### 2.3. Flux Calibration

The extracted one-dimensional spectra were put on an absolute flux scale by reference to spectra of bright A0 stars observed each night at approximately the same airmass as the galaxies and with the same instrumental configuration. In some cases the stellar spectra were additionally recorded through a wide slit, so as to verify empirically the slit losses with the standard set-ups described at §2.1. The stars, which typically have  $K, H \simeq 7$ , were selected from the list of UKIRT photometric standards<sup>4</sup> (see also van der Bliik, Manfroid, & Bouchet 1996). The conversion factor (as a function of wavelength) between counts and flux (in Jy units) was based on the spectral energy distribution of Vega (Colina, Bohlin, & Castelli 1996) and the measured broad band  $K$  and  $H$  magnitudes of the A stars. Since the spectra of A0 stars are relatively smooth at the wavelengths of interest here, they were also used to correct for atmospheric absorption (although in only a few cases did the nebular emission lines fall near telluric features).

It is important to assess the overall reliability of the spectrophotometric calibration—a notoriously difficult step in the reduction of narrow-slit spectra—because it impacts directly on the comparison at §4 below between Balmer line and UV continuum luminosities, and on the abundance determinations in §5. Observations of different A0 stars (on the same night and on different nights) indicate a random uncertainty of  $\leq 15\%$  ( $1\sigma$ ) in the zero point of the flux calibration. However, we are more concerned with systematic errors which may result from inaccurate placing of the targets in the spectrograph slit and from finite aperture effects. Generally, we do not expect the latter to be very large given that the typical half-light radius of Lyman break galaxies in the rest-frame optical is 0.2–0.4 arcsec (Giavalisco, Steidel, & Macchetto 1996; Dickinson 2000; Calzetti & Giavalisco 2000), but see §6 below. We have two ways to check on such systematics. One is to compare observations of the same object obtained with different telescopes. Out of the present sample, Q0201+113 C6 was observed in the  $K$ -band with three different instruments: NIRSPEC on Keck II, ISAAC on VLT, and CGS4 on UKIRT. The three measurements of [O III]  $\lambda 5007$  at  $z = 3.0548$ , respectively ( $4.2 \pm 0.4$ ), ( $7.1 \pm 0.9$ ), and ( $4.6 \pm 0.9$ ) in units of  $10^{-17} \text{ erg s}^{-1} \text{ cm}^{-2}$ , are within  $\sim 2\sigma$  of one another.<sup>5</sup> In a separate test, for two objects where a continuum signal is clearly detected in our NIRSPEC spectra—West MMD11 (Figure 4) and SSA22a D3—we can compare it directly with the broad-band  $K$  magnitude (Table 1). In both cases we find that the spectra underestimate the continuum flux by the same factor of 1.4. We intend to continue monitoring the issue of spectrophotometric accuracy as our survey progresses. On the basis of these limited tests it appears that our absolute fluxes may be in error by up to about 50%. We shall take this uncertainty into account in the analysis of our results.

---

<sup>4</sup>Available at <http://www.jach.hawaii.edu/JACpublic/UKIRT/astronomy/calib>

<sup>5</sup>As explained in §3.1 below, this line was misidentified as [O III]  $\lambda 4959$  at  $z = 3.094$  in the CGS4 spectrum analyzed by Pettini et al. (1998).

### 3. Comments on Individual Objects

From Figures 1–3 it can be readily realized that the rest-frame optical spectra of the Lyman break galaxies in the present sample share many similarities. The spectra are dominated by the strong nebular lines, as is the case in local H II galaxies, and the rest-frame blue continuum is generally too weak to be detected. There is a remarkable uniformity in the line widths (as we shall see at §6 below, the one dimensional velocity dispersion is between  $\sigma = 50$  and  $115 \text{ km s}^{-1}$ ), and in the relative line strengths, with  $\text{H}\beta$  generally weaker, or at most as strong as,  $[\text{O III}]\lambda 4959$ . This probably explains why  $\text{H}\beta$  is undetected in most of our ISAAC spectra which, because of their higher dispersion and the smaller aperture of the VLT, generally have a higher detection threshold than the NIRSPEC spectra. If these line ratios are typical of most galaxies at  $z \simeq 3$ ,  $[\text{O III}]\lambda 5007$  is then the most prominent spectral feature to fall in near-IR wavelength region, rather than  $\text{H}\alpha$ . The generally high excitation of the H II gas is further reflected by the weakness of  $[\text{O II}]\lambda 3727$  relative to  $[\text{O III}]\lambda 5007$  in all five cases observed; compounded with the higher density of strong sky lines in the  $H$ -band, this makes  $\lambda 3727$  a difficult feature to detect, as can be appreciated by comparing Figure 3 with Figures 1 and 2. Thus the prospects for using  $[\text{O II}]$  to probe galaxies at  $z > 4$ , where  $[\text{O III}]$  and  $\text{H}\beta$  are redshifted beyond the  $K$ -band, are not encouraging even with 8-10 m telescopes.

Before discussing further the properties of the sample as a whole, we comment briefly on a few objects.

#### 3.1. Comparison with UKIRT Observations

We reobserved two galaxies out of the five in the sample by Pettini et al. (1998), Q0201+113 C6 and DSF 2237+116a C2 (the latter shown in the bottom panel of Figure 1). With the better spectra now available we realize that the spectral features in the former were misidentified, and the emission line redshift (vacuum heliocentric) is  $z_{\text{H II}} = 3.0548$  rather than 3.094 as reported earlier. The confusion arose because we incorrectly identified  $[\text{O III}]\lambda 5007$  as  $\lambda 4959$  and a noise feature as  $\text{H}\beta$ . The new value of redshift is in much better agreement with that of the interstellar absorption lines in the rest-frame UV, thereby removing the anomaly noted by Pettini et al. In the case of DSF 2237+116a C2, we confirm the redshift, but not the strengths and widths of the emission lines. In the CGS4 data this galaxy appeared to have lines twice as strong and wide as those of the other four objects observed, although we did express concerns about possible noise contamination. The values measured from the much higher signal-to-noise ratio NIRSPEC spectrum,  $\sigma = 100 \text{ km s}^{-1}$ ,  $W_{\text{H}\beta} = 25 \text{ \AA}$  (rest frame equivalent width), and  $W_{5007} = 128 \text{ \AA}$ , are smaller by about a factor of 2 than those reported in Pettini et al, bringing this galaxy in line with the rest of the sample.



### 3.2. Null Detections

Out of the 15 LBGs targeted by our survey so far, 13 have yielded detections of nebular emission lines. The two objects where no signal could be found in the reduced two-dimensional spectra are Q1422+231 D78 and DSF 2237+116b C21 (see Table 1). The latter was observed in poor seeing conditions; furthermore it is the highest redshift object in the present sample, placing [O III]  $\lambda$ 5007 at  $2.2 \mu\text{m}$  where the thermal background at Paranal is more than five times higher than at  $2.0 \mu\text{m}$ . The redshift of the former is uncertain and may have been misidentified. Another possibility is that these are objects caught in a post-starburst phase, when the emission lines have faded but the UV continuum remains bright. From these limited statistics we conclude that the fraction of bright LBGs in a post-starburst phase is at most  $\sim 13\%$ .

### 3.3. Q0256–000 C17

In this case we were surprised to find *two* emission line spectra along the slit, one at the position of the LBG and the other displaced by 3.15 arcsec to the NW (see Figure 14 of Cuby et al. 2000). The two spectra, reproduced in the middle two panels of Figure 2, are similar but not identical; in particular the second set of lines (Q0256–000 C17b) is blueshifted by  $42 \text{ km s}^{-1}$  relative to the first. In our cosmology the spatial separation between the two emitting regions corresponds to a projected distance of  $24h_{70}^{-1} \text{ kpc}$ . Upon re-examination of our broad-band images, we can see a very faint object at the position of this second [O III] emitter with  $\mathcal{R} = 25.97$  (below our magnitude limit for selecting *U*-drop candidates),  $(G - \mathcal{R}) = 0.86$ , and  $(U_n - G) > 1.2$ . With the assumption that the mean  $\langle \mathcal{R} - K_{\text{AB}} \rangle = 0.74$  of the present sample applies to Q0256–000 C17b too (see §4 below), we deduce a rest frame equivalent width  $W_{5007} = 630 \text{ \AA}$ . While relatively rare, H II galaxies with such a high equivalent width of [O III]  $\lambda$ 5007 are not unknown locally; for example, in the catalog by Terlevich et al. (1991) 31 out of 425 emission line galaxies have  $630 \leq W_{5007} \leq 2500 \text{ \AA}$ .

### 3.4. West MMD11

Among the objects observed is West MMD11, one of the few LBGs to have been detected at sub-mm wavelengths with SCUBA (Chapman et al. 2000). This object has unusually red optical-UV colors; with  $\mathcal{R} - K_{\text{AB}} = 2.72$  it stands out from the rest of the sample in Table 1 which has  $\langle \mathcal{R} - K_{\text{AB}} \rangle = 0.74 \pm 0.35 (1\sigma)$ . As can be seen from Figure 4, our NIRSPEC observations clearly show the rest frame optical continuum, only detected in one other object, SSA22a D3. However, it can also be readily appreciated from Figure 4 that the emission line spectrum of West MMD11 is in no way atypical; the strengths and widths of [O III] and H $\beta$ , as well as their ratio, are similar to those of the other galaxies in our sample (see also Tables 2 and 4, and Figures 5 and 8 below). As pointed out by Adelberger & Steidel (2000), the unusually red color of

West MMD11 cannot be entirely attributed to dust extinction, a conclusion consistent with the findings reported here. Perhaps the optical continuum is indicative of an earlier strong burst of star formation, well separated in time from the one which produced the OB stars we now see in the UV continuum and H II region emission lines.

### 3.5. Other Objects in Table 1

When considering the near-IR properties of Lyman break galaxies in §4–6 below, we have expanded the present sample of 15 objects with published observations for an additional four. Two, Q0000–263 D6 and B2 0902+343 C6, are from our earlier UKIRT work; although these data have to be considered as tentative, given the discussion at §3.1 above, we note that the relevant measurements are typical of the rest of the sample. Our conclusions would remain unaltered if we excluded these two galaxies from the analysis. The other two LBGs, West CC13 and MS 1512-cB58, have been observed in the *K*-band with NIRSPEC by Teplitz et al. (2000a,b respectively) using a similar instrumental setup as that described at §2.1 above, although the integration times were shorter than those of our own observations. Other relevant details are given in Table 1.

## 4. Star Formation Rates and Dust Extinction

Up to now most estimates of the star formation activity in galaxies at  $z \simeq 3$  have been obtained from consideration of their ultraviolet continuum luminosity. In the *K*-band we have access to another star formation rate indicator in the H $\beta$  line. Apart from the obvious importance of measuring a physical quantity in two independent ways, there are at least two additional incentives to comparing UV and Balmer line luminosities. First, many of the surveys at lower redshifts have been based on H $\alpha$  (e.g. Gallego et al. 1995; Salzer et al. 2000; Tresse & Maddox 1998; Glazebrook et al. 1999; Yan et al. 1999; Moorwood et al. 2000); clearly, it is desirable to use the same measure (or two closely related ones such as H $\alpha$  and H $\beta$ ) when considering the evolution with redshift of global properties such as the volume averaged star formation rate density. Second, almost by definition, all interstellar reddening curves rise from the optical to the ultraviolet. Thus, at least in principle, it should be possible to deduce the degree of extinction from the comparison between the values of star formation rate deduced from the UV continuum and from the Balmer lines.

Data relevant to this comparison are collected in Table 2. In our enlarged sample there are 14 LBGs where we either detect the H $\beta$  emission line or can place a useful upper limit to its flux. In columns (6)–(8) of Table 2 we list respectively the measured H $\beta$  fluxes, rest frame equivalent widths, and luminosities. The values of equivalent width were derived by referring the measured

line fluxes to the continuum fluxes implied by the broad-band  $K_{AB}$  magnitudes<sup>6</sup> according to the standard relation:

$$AB = -48.60 - 2.5 \log f_\nu \quad (1)$$

where  $f_\nu$  is the flux in units of  $\text{erg s}^{-1} \text{cm}^{-2} \text{Hz}^{-1}$ . In four cases where a  $K$ -band magnitude is not available, we adopted the mean  $\langle \mathcal{R} - K_{AB} \rangle = 0.74 \pm 0.35$  ( $1\sigma$ ) for the sample (excluding West MMD11 as discussed at §3.4 above). The UV continuum luminosities at  $1500 \text{ \AA}$  listed in column (5) were calculated from the  $\mathcal{R}$  magnitudes in column (3) also using eq.(1) and applying, where necessary,  $k$ -corrections deduced from the continuum slope measured in our LRIS spectra. Since the effective wavelength of our  $\mathcal{R}$  filter,  $6850 \text{ \AA}$ , corresponds to a rest frame wavelength of  $1670 \text{ \AA}$  at the median  $z = 3.1$ , the required  $k$ -corrections were normally less than 10%. Finally, columns (9) and (10) of Table 2 give the the star formation rates implied by the  $H\beta$  and UV continuum luminosities listed in columns (8) and (5) respectively, adopting Kennicutt’s (1998) calibrations:

$$\text{SFR}(M_\odot \text{yr}^{-1}) = 1.4 \times 10^{-28} L_{\text{FUV}}(\text{erg s}^{-1} \text{Hz}^{-1}), \quad (2)$$

$$\text{SFR}(M_\odot \text{yr}^{-1}) = 7.9 \times 10^{-42} L_{\text{H}\alpha}(\text{erg s}^{-1}), \quad (3)$$

and assuming a ratio  $H\alpha/H\beta = 2.75$  (Osterbrock 1989). Both transformations are appropriate to continuous star formation with a Salpeter initial mass function (IMF) between  $0.1$  and  $100 M_\odot$ ; we note that eq. (2) gives values of SFR 40% higher than the calibration we adopted in Pettini et al. (1998). More generally, both conversions from luminosity to SFR are subject to significant uncertainties, as discussed by Kennicutt (1998) and more recently re-emphasized by Charlot & Longhetti (2001). However, here we are concerned mainly with *comparing* the values of SFR deduced from these two indices; since they both trace massive stars the hope is that many of the systematic uncertainties may be reduced when considering the ratio  $\text{SFR}_{H\beta}/\text{SFR}_{\text{UV}}$ .

Nevertheless, several qualifications are necessary before proceeding further. First, the conversion factor  $H\alpha/H\beta = 2.75$  does not take into account corrections to the  $H\beta$  flux for reddening and stellar absorption. We suspect that both are likely to be of secondary importance, however. The values of  $E(B - V)$  implied by the slopes of the UV continua of most Lyman break galaxies correspond to small Balmer decrements; for example in MS 1512-cB58, which with  $E(B - V) \simeq 0.3$  is among the more reddened LBGs, dust extinction reduces the  $H\beta/H\alpha$  ratio by only  $\sim 10\%$  relative to the recombination value (Teplitz et al. 2000b). The integrated  $H\beta$  stellar absorption line is expected to have an equivalent width  $W_{\text{abs}} \lesssim 5 \text{ \AA}$  (Kobulnicky, Kennicutt, & Pizagno 1999) and is therefore likely to result in a small correction (comparable to the statistical error) for all the entries in Table 2, except for the two cases where we measure  $W_{H\beta} < 10 \text{ \AA}$ . A potentially more serious effect which may lead us to underestimate  $\text{SFR}_{H\beta}$  relative to  $\text{SFR}_{\text{UV}}$  is light loss through the spectrograph slit, since the former is derived from a spectrophotometric measurement whereas

---

<sup>6</sup>The emission lines themselves make a negligible contribution to  $K_{AB}$

the latter is from broad-band photometry. Our limited internal checks described at §2.3 above suggest that such an underestimate may be less than  $\sim 50\%$ , although future observations may lead to a revised figure.

With these reservations in mind, we compare the two sets of measurements of SFR in Figure 5, where the ratio  $\text{SFR}_{\text{H}\beta}/\text{SFR}_{\text{UV}}$  is plotted against the *intrinsic* far-UV spectral slope. The most reliable measure of the latter, free from the uncertainties inherent in narrow slit spectrophotometry, is the  $(G - \mathcal{R})$  color, corrected for the opacity of the Lyman  $\alpha$  forest according to the statistical prescription of Madau (1995). Values of  $(G - \mathcal{R})_{\text{corr}}$  are tabulated in column (4) of Table 2;  $(G - \mathcal{R})_{\text{corr}} = 0.0$  and  $1.0$  correspond to a UV spectral index  $\beta = -2$  and  $+0.6$  respectively, when the spectrum is approximated by a power law of the form  $F_\lambda \propto \lambda^\beta$ .

It can be readily realized from Figure 5 and Table 2 that the values of SFR deduced from  $\text{H}\beta$  and from the far-UV continuum agree within a factor of  $\sim 2$  in nearly every case. There is no tendency for  $\text{SFR}_{\text{H}\beta}$  to be systematically greater than  $\text{SFR}_{\text{UV}}$ , nor any evidence for the ratio of these two quantities to be higher in galaxies with a redder UV continuum. Earlier suggestions of such a trend in samples of only a few objects (Pettini et al. 1998; Teplitz et al. 2000a) now appear to have been the artifact of small number statistics<sup>7</sup>.

In approximately half of the cases we find  $\text{SFR}_{\text{H}\beta} \lesssim \text{SFR}_{\text{UV}}$ . Apart from the caveats expressed above, there are several plausible explanations for this apparently surprising result. Even without appealing to differences in the IMF, the Balmer lines are expected to vary on shorter timescales than the UV continuum if ‘continuous’ star formation is in reality an approximation to a series of individual starburst episodes (Glazebrook et al. 1999; Bunker, Moustakas, & Davis 2000). This is because the overwhelming contribution to the ionizing flux reprocessed in the Balmer lines is from the most massive stars, at the very tip of the IMF, while a wider range of stellar masses produces the continuum at  $1500 \text{ \AA}$ . In this scenario, LBGs with  $\text{SFR}_{\text{H}\beta} < \text{SFR}_{\text{UV}}$  are galaxies observed 5–10 Myr after a major star formation event. Other possibilities include higher reddening of the Balmer lines than the UV continuum, again related to the different evolutionary timescales of the stars involved (Calzetti 1997), and the leakage of some of the Lyman continuum photons from the galaxies (Steidel, Pettini & Adelberger 2001). In this respect Lyman break galaxies at  $z \simeq 3$  are actually not dissimilar to UV selected galaxies at lower redshifts, where recent comprehensive studies have shown that  $\text{H}\alpha$  and the UV continuum are qualitatively consistent with each other, although generally at lower luminosities than those of the present high- $z$  sample (Sullivan et al. 2000; Bell & Kennicutt 2001). In any case, the simplest conclusion from the results in Figure 5 is that, for the Lyman break galaxies in the present sample (which is representative of the range of  $(G - \mathcal{R})$  colors of our full survey), the higher extinction at UV wavelengths predicted by all reddening curves is evidently masked by the uncertainties discussed above in relating UV continuum and  $\text{H}\beta$  luminosities. The differential extinction between the continuum at  $1500 \text{ \AA}$  and

---

<sup>7</sup>The apparent trend in Figure 5 of Pettini et al. (1998) was due to a single object, DSF 2237+116a C2, whose  $\text{H}\beta$  flux we have now revised downward by a factor of  $\sim 3$  (§3.1).

$H\beta$  must therefore be relatively small, as indeed expected on the basis of the reddening ‘recipe’ by Calzetti (1997).

In concluding this section, we point out that our results contradict two commonly held views. First, it is often stated that the UV continuum is an unreliable measure of the SFR and that the Balmer lines are to be preferred, partly because they suffer less extinction and partly because they have been studied in much larger samples of nearby galaxies. However, adding up the entries in columns (9) and (10) of Table 2 (and taking the upper limits as detections) we find that, for the 14 Lyman break galaxies considered here, the total values of  $SFR_{H\beta}$  and  $SFR_{UV}$  are within 15% of each other. Thus both SFR indicators, *uncorrected for dust extinction*, give essentially the same star formation rate density. Secondly, it is felt by some that the relative strengths of the Balmer lines give a more secure estimate of the colour excess  $E(B - V)$  than the slope of the far-UV continuum. However, as we have seen, in most LBGs at  $z \simeq 3$  the Balmer decrement is too small to be measured with the required precision from ground-based IR spectroscopy, whereas the UV spectral index  $\beta$  can be readily obtained from broad-band optical photometry.

## 5. The Oxygen Abundance

Measurements of element abundances in high redshift galaxies hold powerful clues to their evolutionary status, to their links with today’s galaxy populations, and to the onset of star formation in the universe. Up to now progress on these issues has relied almost exclusively on studies of damped Lyman  $\alpha$  systems (e.g. Pettini et al. 1999; Ellison et al. 2001; Prochaska, Gawiser, & Wolfe 2001 and references therein) which, however, generally do not probe the most active star forming sites (e.g. Bunker et al. 1999; Kulkarni et al. 2000, 2001 and references therein). In contrast, we are still essentially ignorant of the degree of metal enrichment reached by Lyman break galaxies. Yet these objects could be important contributors to the census of metals at high redshifts which currently seems to show a marked deficit—so far we can account for only about 1/10 of the element production associated with the UV light density at  $z \gtrsim 3$  (Pettini 1998; Pagel 2000).

To date there is only one LBG where element abundances have been determined with some degree of confidence, the gravitationally lensed galaxy MS 1512-cB58 at  $z = 2.7290$ , where young stars, H II regions, and neutral interstellar gas all exhibit a metallicity of about 1/3 solar (Pettini et al. 2000; Teplitz et al. 2000b; Leitherer et al. 2001). Here we provide measurements for an additional four LBGs, albeit of lower accuracy than allowed by the gravitationally lensed nature of MS 1512-cB58.

Approximate estimates of the oxygen abundance in H II regions have traditionally been obtained from the strong line index  $R_{23}$  which relates (O/H) to the relative intensities of [O II]  $\lambda 3727$ , [O III]  $\lambda \lambda 4959, 5007$ , and  $H\beta$  (Pagel et al. 1979). Kobulnicky et al. (1999) have

recently re-examined the accuracy of this method when applied to the integrated spectra of distant galaxies and in doing so addressed a number of potential problems including the effects of abundance gradients, inhomogeneous temperature and ionization, stellar absorption and other complications. They concluded that, given spectra of sufficient signal-to-noise ratio,  $R_{23}$  typically measures the abundance of oxygen to within  $\pm 0.2$  dex.

Measurements in the four galaxies in our sample for which we cover all four emission lines are collected in Table 3. Values of  $R_{23} \equiv (F_{5007} + F_{4959} + F_{3727})/F_{H\beta}$  are listed in column (9); the range reflects the statistical  $1\sigma$  errors in the individual values of  $F$ . Again, we made no attempts to correct the observed fluxes for differential extinction because we expect this to be a small effect compared with other uncertainties. In deriving the oxygen abundances we made use of the most recent formulation by Kobulnicky et al. (1999) of the analytical expressions by McGaugh (1991); these formulae express (O/H) in terms of  $R_{23}$  and the ionization index  $O_{32} \equiv (F_{5007} + F_{4959})/F_{3727}$ . The results are illustrated in Figure 6 which shows the well-known double-valued nature of the relation. In the last two columns of Table 3 we list separately the values of (O/H) for the lower and upper branches; in each column the range of values includes the statistical uncertainties in both  $R_{23}$  and  $O_{32}$ . We also include in the table the results by Teplitz et al. (2000b) for MS 1512-cB58.<sup>8</sup>

It can be seen from these data that Lyman break galaxies generally tend to lie toward the right-hand side of the diagram with values  $\log R_{23} \gtrsim 0.7$ . In four out of five cases (the exception being Q0201+113 C6) the statistical errors in the emission line ratios are tolerable, leading to an uncertainty in (O/H) of only about a factor of two. Much more serious is the ambiguity resulting from the double-valued nature of the relationship between (O/H) and  $R_{23}$ . Only in one case, SSA22a D3, do we measure a value of  $R_{23}$  which falls in an unequivocal region of the diagram and deduce (O/H) = 8.04–8.55, (between 1/6 and 1/2 of solar). More generally, the two possible solutions differ by nearly one order of magnitude; oxygen could be as abundant as in the interstellar medium near the Sun, where  $(\text{O}/\text{H})_{\text{ISM}} = 2/3 (\text{O}/\text{H})_{\odot}$  (Meyer, Jura, & Cardelli 1998; Esteban et al. 1998) or as low as in low luminosities H II galaxies at  $\approx 1/10$  solar.

This unsatisfactory state of affairs can in principle be resolved by observing the [N II]  $\lambda\lambda 6548, 6584$  and  $H\alpha$  emission lines; the secondary nature of nitrogen leads to a strong dependence of the [N II]/ $H\alpha$  intensity ratio on (O/H) (Kobulnicky et al. 1999; Terlevich, Denicolo, & Terlevich 2001). It was on this basis that Teplitz et al. (2000b) concluded that MS 1512-cB58 lies on the upper branch of (O/H) vs.  $R_{23}$  relation, and the resulting  $(\text{O}/\text{H}) \approx 1/3 (\text{O}/\text{H})_{\odot}$  does indeed agree with the abundances of other elements measured in OB stars and H I gas.

---

<sup>8</sup>We note in passing that, as pointed out most recently by Pilyugin (2000), the calibration by McGaugh (1991) overestimates the upper branch value of (O/H) by about 0.2 dex when compared with the empirical best fit to accurate abundances determined from temperature sensitive line ratios. However, the analytical expressions given in Kobulnicky et al. (1999) partly compensate for this effect.

The fact that for two objects (MS 1512-cB58 and SSA D3) it has been possible to determine with some degree of confidence that the oxygen abundance is relatively high is in our view insufficient ground to assume that this is *generally* the case in Lyman break galaxies (e.g. Teplitz et al. 2000a; Kobulnicky & Koo 2000). Although we see a great deal of uniformity in the ratio of [O III]/H $\beta$  among all the LBGs observed (Figures 1 and 2), the normally high values of  $R_{23}$  implied could still hide a substantial spread in (O/H), as demonstrated by Figure 6. The only reliable conclusions we can draw are that the Lyman break galaxies in our sample: (a) do not have super-solar abundances and (b) are significantly more metal-rich than damped Lyman  $\alpha$  systems at the same epoch, since the latter typically have metallicities  $Z \approx 1/30 Z_{\odot}$  at  $z \simeq 3$  (Pettini et al. 1999; Prochaska et al. 2001). If either of these two statements were incorrect, then we would expect  $\log R_{23} \leq 0.5$  which can already be excluded by the measured [O III]/H $\beta$  ratios without recourse to [O II]  $\lambda 3727$ .

The inclusion of [N II] and H $\alpha$  in the abundance analysis is generally not an option (at least from the ground) for galaxies at  $z \simeq 3$  where the [N II] doublet and H $\alpha$  lines are redshifted beyond the  $K$ -band. Even at more favourable redshifts near  $z = 2.3$  for example, where all the transitions of interest fall within atmospheric transmission windows, the determination of nebular abundances in Lyman break galaxies remains a difficult task. First, there will be relatively few cases where the full complement of [O II], H $\beta$  [O III], H $\alpha$ , and [N II] lines is well clear of OH sky emission. Second, recording all the lines in the three near-IR bands with sufficient resolution and S/N will require nearly one night of observations on an 8-10 m class telescope for a single LBG. Thus it appears that, even when multi-object IR spectrographs become available, assembling a moderately large sample of (O/H) measurements at high redshifts will involve a major observational effort. There is therefore a strong incentive to explore alternative abundance indicators in the rest-frame UV region which is more easily studied from the ground (e.g. Leitherer et al. 2001).

### 5.1. Metallicity-Luminosity Relation

Present-day galaxies exhibit a clear trend between  $B$ -band luminosity and the oxygen abundance of their H II regions (e.g. Skillman, Kennicutt, & Hodge 1989). This metallicity-luminosity relation extends across morphological types and over 9 magnitudes in luminosity, and appears to hold at least back to  $z \simeq 0.4$  (Kobulnicky & Zaritsky 1998). Presumably it reflects the fundamental role which galaxy mass plays in determining the degree of chemical enrichment of the interstellar medium, through either the rate at which elements are produced by star formation, or the ease with which they can escape the gravitational potential of the galaxy (or both). It is clearly of interest to assess whether Lyman break galaxies conform to this relation. We address this question in Figure 7, where the low redshift points are from the compilation by Kobulnicky & Koo (2000) after adjustment to our cosmology (we refer the reader to that paper for references to the individual sets of measurements). The box showing the location of the Lyman break galaxies encompasses the range of values of (O/H) determined for the five LBGs above, and the range of

rest-frame  $B$ -band luminosities for the *full* sample (excluding West MMD11 which is atypical). Values of  $M_B$  were deduced from the observed (or estimated)  $K$ -band magnitudes and are listed in column 4 of Table 4 in §6.1 below.<sup>9</sup>

It is evident from Figure 7 that LBGs at  $z \simeq 3$  do not conform to today’s metallicity-luminosity relation, as already noted by Kobulnicky & Koo (2000). Even allowing for the uncertainties in the determination of (O/H) discussed above, LBGs fall below the local line of best fit and have much lower oxygen abundances than expected for their luminosities. This is a secure statement; for our objects to fall on the line, their metallicities would have to be well above solar. In this regime  $F_{H\beta} > F_{[\text{O III}]}$  ( $\log R_{23} < 0$  in Figure 6), as is the case in present-day nuclear starbursts (Ho, Filippenko, & Sargent 1997), whereas in *all* our galaxies  $F_{H\beta} \ll F_{[\text{O III}]}$ . The most obvious interpretation of this result is that Lyman break galaxies have mass-to-light ratios which are significantly lower than those which apply to the normal galaxy population at the present epoch (see also §6.1 below). In this respect, they are more extreme examples of today’s H II galaxies, which also tend to lie below the line of best fit in Figure 7. Another possibility is that the whole metallicity-luminosity relation is displaced to lower abundances at high redshifts, when the universe was younger and the total interval of time available for the accumulation of the products of stellar nucleosynthesis was shorter. It should be possible to determine the magnitude of this second effect by measuring the oxygen abundance in known samples of galaxies at  $z \simeq 1$ , a project which is within the capabilities of current instrumentation.

## 6. Kinematics

### 6.1. Velocity Dispersions

The one parameter which is most easily measured from our data is  $\sigma$ , the one dimensional velocity dispersion of the H II gas along the line of sight, since all that is required is the detection of one line (usually [O III]  $\lambda 5007$ ). Accordingly, this is the physical quantity for which we have the most extensive set of values, 16 in total. They are listed in column (7) of Table 4 (after correction for the instrumental broadening) and plotted in Figure 8 vs. the far-UV and  $B$ -band luminosities (deduced from the observed  $\mathcal{R}$  and  $K$  magnitudes as explained in §4 and §5.1 respectively). It can be seen from the Table and Figure that the galaxies in our sample exhibit a relatively narrow range of values of  $\sigma$ , between  $\sim 50$  and  $\sim 115 \text{ km s}^{-1}$ . The median value is  $\sigma \simeq 70 \text{ km s}^{-1}$ .

In Pettini et al. (1998) we used the velocity dispersions of the nebular lines to estimate the masses of the LBGs observed; the enlarged data set available now essentially confirms the

---

<sup>9</sup>Strictly speaking, at the median  $z = 3.1$  the observed  $K$ -band corresponds to wavelengths between rest-frame  $B$  and  $V$ . However, the small  $k$ -corrections to rest-frame  $B$  (Shapley et al. in preparation) are unimportant for the purpose of the present discussion.



conclusion of that work that  $M > 10^{10} M_{\odot}$ . In the idealized case of a sphere of uniform density,

$$M_{\text{vir}} = 5 \times \sigma^2 r_{1/2} / G \quad (4)$$

or

$$M_{\text{vir}} = 1.2 \times 10^{10} M_{\odot} \frac{\sigma^2}{100 \text{ km s}^{-1}} \frac{r_{1/2}}{\text{kpc}} \quad (5)$$

where  $G$  is the gravitational constant and  $r_{1/2}$  is the half-light radius. *HST* images of Lyman break galaxies obtained with WFPC2 and NICMOS show that they typically have  $r_{1/2} = 0.2\text{--}0.4$  arcsec, irrespectively of whether they are observed in the rest-frame UV or optical light (Giavalisco et al. 1996; Dickinson 2000; Calzetti & Giavalisco 2000). In our cosmology,  $r_{1/2} = 0.3$  arcsec corresponds to  $2.3 h_{70}^{-1}$  kpc and the median  $\sigma = 70 \text{ km s}^{-1}$  therefore translates to  $M_{\text{vir}} \simeq 1.3 \times 10^{10} h_{70}^{-1} M_{\odot}$ .

A similar value would result for a disk-like geometry. Extensive simulations by Rix et al. (1997), including random orientation and other effects, have shown that  $\sigma \approx 0.6 \times V_c$ , where  $V_c$  is the maximum circular velocity of the ionized gas. Since presumably  $V_c$  is reached at radii  $r \geq r_{1/2}$ , the enclosed dynamical mass  $M_{\text{dyn}} = V_c^2 \times r / G$  is not very different from the value of  $M_{\text{vir}}$  obtained from eq.(5). It is likely, however, that these masses do not reflect the whole gravitational potential of the galaxies but rather refer mainly to the central, high surface brightness regions. Locally, it is found that in nuclear starbursts and blue compact galaxies the optical emission lines do not span the full extent of the rotation curve traced by the 21 cm line of H I (Lehnert & Heckman 1996; Pisano et al. 2001).

When combined with the median  $M_B = -22.60$  of our sample (uncorrected for extinction), the above mass estimate  $M \simeq 1.3 \times 10^{10} M_{\odot}$  implies mass-to-light ratios  $M/L \approx 0.15$  in solar units. Not surprisingly, this value is much lower than those measured in the inner regions of galaxies today, which are in the range 2 – 10 (e.g. Binney & Tremaine 1987). Note that this increase in luminosity for a given mass by a factor of  $\approx 30$ —or 3.7 magnitudes in  $M_B$ —is similar to the horizontal offset of LBGs from today’s metallicity-luminosity relation shown in Figure 7. Thus, our galaxies seem to have mass-to-light ratios typical of young stellar populations. From the *Starburst99* models of Leitherer et al. (1999), adjusted to a lower mass limit  $M_{\text{low}} = 0.1 M_{\odot}$ , we find that  $M/L = 0.15$  is intermediate between the values appropriate to continuous star formation lasting for  $10^8$  ( $M/L = 0.05$ ) and  $10^9$  ( $M/L = 0.23$ ) years. This result is in good agreement with the conclusion by Shapley et al. (in preparation) that the optical to near-IR spectral energy distributions of most LBGs in their sample are indeed indicative of ages between  $10^8$  and  $10^9$  years.

Nevertheless, it remains to be established whether in Lyman break galaxies at  $z = 3$  the line widths we measure do reflect mostly the overall velocity dispersion among different star-forming regions—the underlying assumption to using them as tracers of mass—as opposed to being dominated by outflows and other large-scale motions of a non-gravitational origin (see §6.3 below). It is evident from Figure 8 that there no correlation between velocity dispersion and either UV or optical luminosity. While it could be argued that any such trend would be difficult to discern given

the small sample size and the narrow range of absolute magnitudes probed, we are struck by the results of Adelberger et al. (in preparation). Their much larger (several hundred) sample of Balmer break galaxies at  $z \simeq 1$  not only exhibits values of  $\sigma$  between  $\sim 50$  and  $\sim 100 \text{ km s}^{-1}$ , similar to those found here, but also shows no correlation between velocity dispersion and luminosity over a range of nearly five magnitudes.<sup>10</sup> Thus, until the physical origin of the broadening of the nebular lines in Lyman break galaxies is clarified, it would be unwise to draw far-reaching conclusions from the mass estimates derived above.

## 6.2. Spatially Resolved Line Profiles

We can try and address this last question with ISAAC observations of two of our objects, Q0347–383 C5 and SSA22a MD46, where we unexpectedly discovered spatially resolved emission along the spectrograph slit. As can be seen from Figures 9 and 10, the [O III] doublet lines are tilted in the 2-D images of these galaxies, hinting at a regular pattern of velocities as may be produced by a rotating disk. A third such case (out of a sample of six objects) has recently been reported by Moorwood et al. (2000) from H $\alpha$  observations of a galaxy at  $z = 2.192$ . However, these authors found larger velocity spreads—and consequently deduced larger masses—than determined here, as we now discuss.

To investigate the kinematics of the ionized gas, we extracted the spectra in intervals of two spatial increments, each 0.146 arcsec on the sky. In this way we optimally sampled the seeing profile which was measured to have FWHM = 0.62 and 0.64 arcsec on the final stacked 2-D images obtained with integration times of 18 000 and 14,400 s for Q0347–383 C5 and SSA22a MD46 respectively.<sup>11</sup> At the redshifts of these two galaxies,  $z = 3.2337$  and 3.0855 respectively, we sample the spatial structure of the emission at projected intervals on the sky of  $2.2h_{70}^{-1} \text{ kpc}$  in our cosmology.

The bottom right-hand panels in Figures 9 and 10 show the runs of relative velocities along the slit, measured from the central wavelengths of [O III]  $\lambda 5007$  by Gaussian fitting. The velocity ranges spanned by the line *centres* are small, only about  $\pm 30$  and  $\pm 40 \text{ km s}^{-1}$  in Q0347–383 C5 and SSA22a MD46 respectively, over linear projected distances of  $\pm 4.5 \text{ kpc}$ . Taken at face value, these measurements would imply much smaller masses than derived at §6.1 above,  $M_{\text{dyn}} \sim 1.3 \times 10^9 h_{70}^{-1} M_{\odot}$ . However, in reality this value is a very conservative lower limit to the enclosed mass of ionized gas because in each case: (a) the line profiles are only just resolved spatially, and the whole ‘rotation curve’ on either side of the center is sampled with only two

---

<sup>10</sup>This result is not necessarily in conflict with the work of Vogt et al. (1997) who found the Tully-Fisher relation to hold, with only mild evolution, out to  $z \sim 1$ . These authors specifically targeted galaxies with disk morphologies for their study, while the Balmer break galaxies selected by Adelberger et al. are a much more heterogeneous sample.

<sup>11</sup>Recall that all the ISAAC observations included a bright star on the spectrograph slit; this stellar spectrum conveniently provides a measure of the seeing and an astrometric reference point.

points<sup>12</sup>; (b) we do not know the inclination angle of the galaxy; and (c) we do not know the orientation of the spectrograph slit relative to the major axis of the galaxy (if we are indeed dealing with disks).<sup>13</sup>

We can check on points (b) and (c) by examining existing high resolution images of these two LBGs. Q0347–383 C5 was part of the WFPC2 sample of Giavalisco et al. (1996)<sup>14</sup>; in Figure 11 we show the image obtained by combining ten dithered 1800 s exposures through the F702W filter (which is a very close match to our  $\mathcal{R}$ ) filter) after ‘drizzling’ onto a master output pixel grid (Fruchter & Hook 1998). Overlaid on the WFPC2 image is the location on the sky of the 1 arcsec wide ISAAC slit. Q0347–383 C5 exhibits an irregular morphology, with a knot of intense UV emission and extensions of lower surface brightness to the north. The horizontal arrows in Figure 11 delimit the location of the [O III] emission which is clearly *not* coincident with the UV light<sup>15</sup>. With hindsight this is not totally unexpected; some possible causes have been considered in §4. Similar differences in the spatial distributions of H II regions and stellar UV continuum have been observed in nearby starburst galaxies, albeit on smaller scales (e.g. Leitherer et al. 1996). Although the spectrograph slit was fortuitously aligned so as to encompass the extended structure revealed by the WFPC2 image, one can hardly interpret such structure as evidence for a rotating disk, or hazard a guess as to the inclination angle on the sky. Furthermore, some of the apparent rotation in Figure 9 may in reality be an instrumental effect caused by the clumpy structure of the galaxy, if knots of peak [O III] emission are centered at different locations *across* the slit.

In Figure 12 we have overlaid the ISAAC slit on a  $K$ -band image of SSA22a MD46 obtained with NIRC as part of the survey by Shapley et al. (in preparation). In this case our IR spectrum missed a second knot of continuum emission which evidently fell outside the spectrograph slit; it would be interesting to repeat the observation with the slit rotated by 90 degrees so as to probe the kinematics of the gas along the apparent elongation axis of this galaxy.

In summary, while in neither case do we find conclusive evidence supporting the hypothesis that the extended [O III] emission traces a rotation curve, these initial results are nevertheless intriguing. Looking ahead, it should be possible to investigate more extensively the velocity and spatial structure of Lyman break galaxies by combining high resolution imaging with spatially resolved spectroscopy; this task will be accomplished most effectively with near-IR spectrographs fed by adaptive optics systems.

---

<sup>12</sup>It is easy to see that, as each sample point is an average over regions with different velocities in a rising rotation curve, the net effect is an underestimate of  $V_c$  since the the emission line intensity decreases from the center of the galaxy.

<sup>13</sup>The slit orientation on the sky was dictated by the location of the offset star relative to the LBG—see §2.1.

<sup>14</sup>The galaxy was labeled 0347–383–N05 in that paper.

<sup>15</sup>In this case we can register precisely the ISAAC 2-D spectrum and the WFPC2 image because they both include the bright QSO Q0347–383 which is located only 26.7 arcsec away from the LBG.

### 6.3. Large-scale Motions

For 17 LBGs we can compare the redshift of the nebular emission lines,  $z_{\text{H II}}$ , listed in column (2) of Table 4, with the redshift of the interstellar absorption lines,  $z_{\text{abs}}$ ; for a subset of 13 objects we can also include in the comparison the redshift of the Lyman  $\alpha$  emission line,  $z_{\text{Ly}\alpha}$ . Values of  $z_{\text{abs}}$  and  $z_{\text{Ly}\alpha}$  can be found in columns (5) and (4) of Table 1 respectively. The former is the mean of all the UV interstellar absorption lines (generally three or more) between 1250 and 1700 Å which could be identified in our LRIS spectra; we refer the reader to Pettini et al. (2000) for a list of the strongest transitions. The latter was measured either by gaussian fitting or from the peak of the emission, depending on the shape of the Lyman  $\alpha$  emission line. If, as a working assumption, we adopt the values of  $z_{\text{H II}}$  as the systemic redshifts of the galaxies, we can convert  $z_{\text{abs}}$  and  $z_{\text{Ly}\alpha}$  to the relative velocities listed respectively in columns (5) and (6) of Table 4 and plotted in Figure 13.

These data reveal a clear pattern in the kinematics of the interstellar medium of Lyman break galaxies when probed with these three different tracers. In three quarters of the objects observed the interstellar absorption lines are blueshifted relative to the H II region emission lines, while in all cases Lyman  $\alpha$  emission is redshifted.  $\Delta v_{\text{IS abs}}$  is typically between  $\sim -200$  and  $\sim -400 \text{ km s}^{-1}$ , with a median value of  $-300 \text{ km s}^{-1}$ ; values of  $\Delta v_{\text{Ly}\alpha}$  span a larger range, from  $\sim +200$  to  $\sim +1100 \text{ km s}^{-1}$ . A similar effect was already evident in the small sample of Pettini et al. (1998); the new data show it to be a characteristic shared by most Lyman break galaxies. There is no evidence for any dependence of these large velocity offsets on either the far-UV or optical luminosities of the galaxies within the  $\sim 2$  magnitude interval in  $M_{1500}$  and  $M_{\text{B}}$  probed by the present study.

The simplest interpretation—and undoubtedly an oversimplification of a more complex physical picture—is that we are seeing galactic scale outflows driven by the mechanical energy deposited by supernovae and stellar winds in these actively star forming galaxies. Presumably the gas seen in absorption in front of the stars is the approaching part of an expanding shell of swept-up material which has a very high optical depth to Lyman  $\alpha$  photons; thus the only Lyman  $\alpha$  emission detectable along our line of sight is from the back of the shell, *behind* the stars, receding at velocities where no foreground absorption takes place. This behavior of the Lyman  $\alpha$  line is commonly seen in local H II galaxies (Kunth et al. 1998) and has been modelled extensively by Tenorio-Tagle et al. (1999) among others. In MS 1512-cB58, where  $\Delta v_{\text{IS abs}} = -390 \text{ km s}^{-1}$ , Pettini et al. (2000) deduced a mass outflow rate  $\dot{M} \simeq 60 M_{\odot} \text{ yr}^{-1}$ , comparable to the star formation rate  $\text{SFR} \simeq 20 M_{\odot} \text{ yr}^{-1}$  (Table 2). Since both the value of SFR and of  $\Delta v_{\text{IS abs}}$  in MS 1512-cB58 are typical of the present sample of LBGs, it would appear that luminous Lyman break galaxies are *generally* the sites of powerful superwinds involving a mass in baryons comparable to that being turned into stars.

In this and many other respects the properties of the superwinds we see at  $z \simeq 3$  are very similar to those observed in nearby starburst galaxies and reviewed extensively by Heckman

(e.g. Heckman 2000). In the local universe they are found in galaxies with high rates of star formation per unit area,  $\Sigma_* \geq 0.1 M_\odot \text{ yr}^{-1} \text{ kpc}^{-2}$ ; this threshold is exceeded by one order of magnitude by the LBGs considered here, which have typical SFR  $\simeq 40 M_\odot \text{ yr}^{-1}$  and half-light radii  $r_{1/2} = 2.3 \text{ kpc}$ . Similar outflow rates and speeds are involved at high and low redshift; Heckman et al. (2000) calculate that the kinetic energy required is  $\approx 10\%$  of the total kinetic energy supplied by the starburst.

Galactic superwinds have several important astrophysical consequences which have already been considered in the review by Heckman (2000); here we limit ourselves to a few comments of particular significance at high redshift. First, the data in Figure 13, and the mass outflow rates they imply, provide a vivid empirical demonstration of the feedback process required to regulate star formation in nearly all theoretical models of galaxy formation (e.g. Efstathiou 2000; Cole et al. 2000). Second, the results of §5 show Lyman break galaxies to be the most metal-enriched structures at  $z \simeq 3$ , apart from QSOs (Pettini 2000). A significant fraction of these metals will probably be lost from the galaxies altogether, since the measured values of  $\Delta v_{\text{IS abs}}$  are comparable to the escape velocities (Heckman 2000; Ferrara, Pettini, & Shchekinov 2000). While it is still unclear how far this metal-enriched gas will travel (Ferrara et al. 2000; Aguirre et al. 2001), there is at least the potential for seeding large volumes around the galaxies with the products of stellar nucleosynthesis. Furthermore, if most of the metals carried away by galactic superwinds remain in a hot phase, yet to be directly observed, this may help solve the puzzle of the missing metals at high redshift (Pettini 1998; Pagel 2000). Third, in any flattened geometry, it is likely that the expanding superbubbles will ‘punch holes’ through the interstellar medium in the direction of the vertical pressure gradient. Such cavities would allow Lyman continuum photons to leak into the IGM. The common occurrence of superwinds in Lyman break galaxies may then provide a plausible explanation for the high escape fraction of ionizing photons suggested by the recent results of Steidel et al. (2001). Thus, the mechanical energy deposited by the star formation episodes themselves may well be the key physical process ultimately responsible for reionizing of the universe at high redshift.

## 7. Summary and Conclusions

We have presented the first results of a spectroscopic survey of Lyman break galaxies in the near infrared, aimed at detecting nebular emission lines of [O II], [O III] and  $\text{H}\beta$  with the NIRSPEC and ISAAC instruments on the Keck and VLT telescopes respectively. Together with observations from the literature, we have constructed a sample of data for 19 LBGs, the largest considered so far. The galaxies are drawn from the bright end of the luminosity function, from  $\sim L^*$  to  $\sim 4 L^*$ . Their near-IR spectra have been analysed to investigate the star formation rates, dust obscuration, oxygen abundances, and kinematics of the normal galaxy population at  $z \simeq 3$ . The main results of this work are as follows.

(1) The LBGs observed form a very uniform sample in their near-IR properties. The spectra are dominated by the emission lines, and the continuum is detected in only two objects, one of which—West MMD11—has an unusually red optical-to-infrared color with  $(\mathcal{R} - K_{\text{AB}}) = 2.72$ . In all cases [O III] is stronger than  $\text{H}\beta$  and [O II]. The line widths span a relatively small range, with values of the one dimensional velocity dispersion  $\sigma$  between 50 and 115  $\text{km s}^{-1}$ .

(2) The star formation rates deduced from the luminosity of the  $\text{H}\beta$  emission line agree within a factor of  $\sim 2$  with the values implied by the continuum luminosity at 1500  $\text{\AA}$  *before any corrections for dust extinction are applied*. There is no trend in the present sample for the former to be larger than the latter, as may have been expected from the shape of all reddening curves which rise from the optical to the UV. Evidently, any such differential extinction must be small compared with the uncertainties in calibrating these two different measures of the SFR. This conclusion is in agreement with the results of similar recent studies of UV-selected star-forming galaxies at  $z \lesssim 1$  and contradicts the commonly held view that the Balmer lines are more reliable star formation indicators than the UV continuum—from our sample one would obtain essentially the same star formation rate density using either method.

(3) In five cases (four new ones and one previously published) we attempted to deduce values of the abundance of oxygen by applying the familiar  $R_{23}$  method which has been extensively used in local H II regions. We found that generally there remains a significant uncertainty, by up to 1 dex, in the value of (O/H) because of the double-valued nature of the  $R_{23}$  calibrator. Thus, in the galaxies observed oxygen could be as abundant as in the interstellar medium near the Sun, or as low as  $\sim 1/10$  solar. While this degeneracy can in principle be resolved by measuring the [N II]/ $\text{H}\alpha$  ratio (and in the one case where this has proved possible values of (O/H) near the upper end of the range are indicated), this option is not normally available for galaxies at  $z \simeq 3$  because the relevant lines are redshifted beyond the  $K$ -band.

Even so, it is still possible to draw some interesting conclusions. First, LBGs are definitely more metal-rich than damped Lyman  $\alpha$  systems at the same epoch, which typically have metallicities  $Z \approx 1/30 Z_{\odot}$ . This conclusion is consistent with the view that DLAs are drawn preferentially from the faint end of the galaxy luminosity function and are not the most actively star forming galaxies, as indicated by essentially all attempts up to now to detect them via direct imaging. Second, LBGs do not conform to today’s metallicity-luminosity relation and are overluminous for their oxygen abundance. This is probably an indication that they have relatively low mass-to-light ratios, as also suggested by their kinematical masses; a further possibility is that the whole (O/H) vs.  $M_{\text{B}}$  correlation shifts to lower metallicities at high  $z$ , when galaxies were younger.

(4) If the emission line widths reflect the relative motions of H II regions within the gravitational potential of the galaxies, the implied masses are of the order of  $10^{10} M_{\odot}$  within half-light radii of  $\sim 2.5$  kpc. This is likely to be a lower limit to the total masses of the galaxies as would be obtained, for example, if we could trace their rotation curves. A more serious

uncertainty, however, is the real origin of the velocity dispersions we measure. We do not see any correlation between  $\sigma$  and galaxy luminosity in either our limited sample nor in an on-going study by some of us of a much larger sample of galaxies at  $z \simeq 1$  which span five magnitudes in luminosity and yet show very similar line widths to those found here. In two cases we have found hints of ordered motions in spatially resolved profiles of the [O III] lines, but attempts to use high resolution images to clarify whether they are indicative of rotating disks proved to be inconclusive.

(5) In all the galaxies observed we find evidence for bulk motions of several hundred  $\text{km s}^{-1}$  from the velocities of the interstellar absorption lines—which are systematically blueshifted—and Lyman  $\alpha$  emission—which is always redshifted—relative to the nebular emission lines. We interpret this effect as indicative of galaxy-wide outflows which appear to be a common characteristic of galaxies with large rates of star formation per unit area at high, as well as low, redshifts. Such ‘superwinds’ involve comparable amounts of matter as is being turned into stars (the mass outflow rate is of the same order as the star formation rate) and about 10% of the total kinetic energy delivered by the starburst. Furthermore, they have a number of important astrophysical consequences. They provide self-regulation to the star formation process; can distribute the products of stellar nucleosynthesis over large volumes (the outflow speeds often exceed the escape velocities); may account for some of the ‘missing’ metals at high redshift; and may also allow Lyman continuum photons to leak from the galaxies into the intergalactic medium, easing the problem of how the universe came to be reionized. On the other hand, the existence of such large velocity fields within Lyman break galaxies makes it difficult to measure precisely their systemic redshifts (as may be required, for example, for detailed clustering studies) unless more than one marker is available.

(6) Finally, we point out some instrumental developments which in our view will greatly aid further progress in this field. In particular, we consider that future spectrographs making use of adaptive optics and incorporating multi-object and integral field facilities will prove to be particularly beneficial for the study of high redshift galaxies at near-IR wavelengths.

We are indebted to the staff of the Paranal and Keck observatories for their expert assistance with the observations. We are especially grateful to Chip Kobulnicky for generously providing the low redshift data shown in Figure 7, for communicating results in advance of publication, and for valuable comments which improved the paper. We acknowledge helpful conversations with Stephane Charlot, Bernard Pagel, and Roberto Terlevich. C.C.S. and K.L.A. have been supported by grants AST 95-96229 and AST 00-70773 from the US National Science Foundation and by the David and Lucile Packard Foundation.

## REFERENCES

- Adelberger, K.L., & Steidel, C.C. 2000, *ApJ*, 544, 218
- Aguirre, A., Hernquist, L., Weinberg, D., Katz, N., & Gardner, J. 2001, *ApJ*, submitted (astro-ph/0006345)
- Bell, E.F. & Kennicutt Jr., R.C. 2001, *ApJ*, in press (astro-ph/0010340)
- Binney, J., & Tremaine, S. 1987, *Galactic Dynamics*, (Princeton:University Press)
- Bunker, A.J., Moustakas, L.A., & Davis, M. 2000, *ApJ*, 531, 95
- Bunker, A.J., Warren, S.J., Clements, D.L., Williger, G.M., & Hewett, P.C. 1999, *MNRAS*, 309, 875
- Calzetti, D. 1997, in *The Ultraviolet Universe at at Low and High Redshift: Probing the Progress of Galaxy Evolution*, ed. W.H. Waller, M.N. Fanelli, J.E. Hollis, & A.C. Danks AIP Conference Proceedings 408, (New York:Woodbury), 403
- Calzetti, D., & Giavalisco, M. 2000, *Ap & Sp Sci*, in press (astro-ph/0012068)
- Chapman, S.C., Scott, D., Steidel, C.C., Borys, C., Halpern, M., Morris, S.L., Adelberger, K.L., Dickinson, M., Giavalisco, M., & Pettini, M. 2000, *MNRAS*, 319, 318
- Charlot, S. & Longhetti, M. 2001, *MNRAS*, in press (astro-ph/0101097)
- Cole, S., Lacey, C.G., Baugh, C.M., & Frenk, C.S. 2000, *MNRAS*, 319, 168
- Colina, L., Bohlin, R., & Castelli, F. 1996, *Absolute Flux Calibration Spectrum of Vega*, STScI Instrument Science Report OSG-CAL-96-01 (Baltimore: STScI)
- Cuby, J.G., Barucci, A., de Bergh, C., Emsellem, E., Moorwood, A.F.M., Petr, M., Pettini, M., & Tresse, L. 2000, *Proc. SPIE*, 4005, 212
- Dickinson, M. 2000, *Philos. Trans. R. Soc. Lond. A*, 358, 2001
- Efstathiou, G. 2000, *MNRAS*, 317, 697
- Ellingson, E., Yee, H.K.C., Bechtold, J., & Elston, R. 1996, *ApJ*, 466, L71
- Ellison, S.L., Pettini, M., Steidel, C.C. & Shapley, A.E. 2001, *ApJ*, 549, in press.
- Esteban, C., Peimbert, M., Torres-Peimbert, S., & Escalante, V. 1998, *MNRAS*, 295, 401
- Ferrara, A., Pettini, M., & Shchekinov, Y. 2000, *MNRAS*, 319, 539
- Fruchter, A.S., & Hook, R.N. 1998, *PASP*, submitted (astro-ph/9808087)



- Gallego, J., Zamorano, J., Aragón-Salamanca, A., & Rego, M. 1995, *ApJ*, 455, L1
- Giavalisco, M., Steidel, C.C., & Macchetto, D. 1996, *ApJ*, 470, 189
- Glazebrook, K., Blake, C., Economou, F., Lilly, S., & Colless, M. 1999, *MNRAS*, 306, 843
- Grevesse, N., & Sauval, A.J. 1998, *Space Sci Rev*, 85, 161
- Heckman, T.M. 2000, in *ASP Conf. Ser., Gas and Galaxy Evolution*, ed. J.E. Hibbard, M.P. Rupen, & J.H. van Gorkom, (San Francisco:ASP), in press (astro-ph/0009075)
- Heckman, T.M., Lehnert, M., Strickland, D., & Armus, L. 2000, *ApJS*, 129, 493
- Ho, L.C., Filippenko, A.V., & Sargent, W.L.W. 1997, *ApJ*, 487, 579
- Kennicutt Jr., R.C. 1998, *ARA&A*, 36, 189
- Kobulnicky, H.A., Kennicutt Jr., R.C., & Pizagno, J.L. 1999, *ApJ*, 514, 544
- Kobulnicky, H.A., & Koo, D.C. 2000, *ApJ*, 545, 712
- Kobulnicky, H.A., & Zaritsky, D. 1998, *ApJ*, 511, 188
- Kulkarni, V.P., Hill, J.M., Schneider, G., Weymann, R.J., Storrie-Lombardi, L.J., Rieke, M.J., Thompson, R.I., & Jannuzi, B.T. 2000, *ApJ*, 536, 36
- Kulkarni, V.P., Hill, J.M., Schneider, G., Weymann, R.J., Storrie-Lombardi, L.J., Rieke, M.J., Thompson, R.I., & Jannuzi, B.T. 2001, *ApJ*, in press (astro-ph/0012140)
- Kunth, D., Mas-Hesse, J.M., Terlevich, E., Terlevich, R., Lequeux, J., & Fall, S.M. 1998, *A&A*, 334, 11
- Lehnert, M.D., & Heckman, T.M. 1996, *ApJ*, 462, 651
- Leitherer, C. 2000, in *A Decade of HST Observations*, ed. M. Livio, K. S. Noll, & M. Stiavelli (Cambridge: CUP), in press
- Leitherer, C., Leão, J.R., Heckman, T.M., Lennon, D.J., Pettini, M., & Robert, C. 2001, *ApJ*, 550, in press
- Leitherer, C., Schaerer, D., Goldader, J.D., González Delgado, R.M., Robert, C., Kune, D.F., de Mello, D.F., Devost, D., & Heckman, T.M. 1999, *ApJS*, 123, 3
- Leitherer, C., Vacca, W.D., Conti, P.S., Filippenko, A.V., Robert, C., & Sargent, W.L.W. 1996, *ApJ*, 465, 717
- Lowenthal, J., et al. 1997, *ApJ*, 481, 673
- Madau, P. 1995, *ApJ*, 441, 18

- McGaugh, S. 1991, *ApJ*, 380, 140
- McLean, I.S., et al. 1998, *Proc. SPIE*, 3354, 566
- Meyer, D.M., Jura, M., & Cardelli, J.A. 1998, *ApJ*, 493, 222
- Moorwood, A.F.M., et al. 1999, *ESO Messenger*, 91, 9
- Moorwood, A.F.M., van der Werf, P.P., Cuby, J.G., & Oliva, E. 2000, *A&A*, 362, 9
- Osterbrock, D.E. 1989, *Astrophysics of Gaseous Nebulae and Active Galactic Nuclei* (Mill Valley:University Science Books)
- Pagel, B.E.J. 2000, in *Galaxies in the Young Universe*, ed. H. Hippelein (Berlin:Springer-Verlag), in press (astro-ph/9911204)
- Pagel, B.E.J., Edmunds, M.G., Blackwell, D.E., Chun, M.S., & Smith, G. 1979, *MNRAS*, 189, 95
- Pettini, M. 1999, in *Chemical Evolution from Zero to High Redshift*, ed. J.R. Walsh, & M.R. Rosa (Berlin:Springer-Verlag), 233
- Pettini, M. 2000, *Philos. Trans. R. Soc. Lond. A*, 358, 2035
- Pettini, M., Ellison, S.L., Steidel, C.C. & Bowen, D.V. 1999, *ApJ*, 510, 576
- Pettini, M., Kellogg, M., Steidel, C.C., Dickinson, M., Adelberger, K.L., & Giavalisco, M. 1998, *ApJ*, 508, 539
- Pettini, M., Steidel, C.C., Adelberger, K.L., Dickinson, M., & Giavalisco, M. 2000, *ApJ*, 528, 96
- Pilyugin, L.S. 2000, *A&A*, 362, 325
- Pisano, D.J., Kobulnicky, H.A., Guzmán, R., Gallego, J., & Bershadsky, M.A. 2001, *ApJ*, submitted.
- Prochaska, J.X., Gawiser, E., & Wolfe, A.M. 2001, *ApJ*, in press
- Rix, H.W., Guhathakurta, P., Colless, M., & Ing, K. 1997, *MNRAS*, 285, 779
- Rousselot, P., Lidman, C., Cuby, J.G., Moorels, G., & Monnet, G. 2000, *A&A*, 354, 1134
- Salzer, J.J., Gronwall, C, Lipovetsky, V.A., Kniazev, A., Moody, J.W., Boroson, T.A., Thuan, T.X., Izotov, Y.I., Herrero, J.L., & Frattare, L.M 2000, *AJ*, 120, 80
- Seitz, S., Saglia, R.P., Bender, R., Hopp, U., Belloni, P., & Ziegler, B. 1998, *MNRAS*, 298, 945
- Skillman, E.D., Kennicutt Jr., R.C., & Hodge, P. 1989, *ApJ*, 347, 875
- Steidel, C.C. 2000, *Proc. SPIE*, 4005, 222
- Steidel, C.C., Adelberger, K.L., Giavalisco, M., Dickinson, M., & Pettini, M. 1999, *ApJ*, 519, 1

- Steidel, C.C., Giavalisco, M., Pettini, M., Dickinson, M., & Adelberger, K.L. 1996, *ApJ*, 462, L17
- Steidel, C.C., Pettini, M., & Adelberger, K.L. 2000, *ApJ*, 546 in press
- Sullivan, M., Treyer, M.A., Ellis, R.S., Bridges, T.J., Milliard, B., & Donas, J. 2000, *MNRAS*, 312, 442
- Tenorio-Tagle, G., Silich, S.A., Kunth, D., Terlevich, E., & Terlevich, R. 1999, *MNRAS*, 309, 332
- Teplitz, H.I., et al. 2000a, *ApJ*, 542, 18
- Teplitz, H.I., et al. 2000b, *ApJ*, 533, L65
- Terlevich, R.J., Denicolo, G., & Terlevich, E. 2001, in
- Terlevich, R., Melnick, J., Masegosa, J., Moles, M., & Copetti, M.V.F. 1991, *A&AS*, 91, 285
- Tresse, L., & Maddox, S.J. 1998, *ApJ*, 495, 691
- van der Blik, N.S., Manfroid, J., & Bouchet, P. 1996, *A&AS*, 119, 547
- Vogt, N.P., Phillips, A.C., Faber, S.M., Gallego, J., Gronwall, C., Guzmán, R., Illingworth, G.D., Koo, D.C., & Lowenthal, J.D. 1997, *ApJ*, 479, L121
- Yan, L., McCarthy, P.J., Freudling, W., Teplitz, H.I., Malmumuth, E.M., Weymann, R.J., & Malkan, M.A. 1999, *ApJ*, 519, L47

TABLE 1  
GALAXIES OBSERVED

Name	RA <sup>a</sup>	Dec <sup>a</sup>	$z_{\text{Ly}\alpha}^b$	$z_{\text{abs}}^c$	$\mathcal{R}$	$(G - \mathcal{R})^d$	$(\mathcal{R} - K_{\text{AB}})^e$	Exp. (s)	Band	Tel./Instrum. & Obs. Run
CDFa D18	00 53 26.7	+12 37 34	3.120:	3.106:	23.74	1.05	...	10 800	<i>K</i>	VLT1/ISAAC Nov. 1999
CDFa C8	00 53 32.9	+12 32 11	...	3.071	23.72	0.96	0.53	9900	<i>K</i>	Keck II/NIRSPEC Sep. 1999
CDFa C1	00 53 34.7	+12 30 30	...	3.111	23.53	0.69	1.11	9000	<i>K</i>	VLT1/ISAAC Sep. 1999
Q0201+113 C6	02 03 41.8	+11 34 42	...	3.053	23.92	0.60	0.57	5400	<i>K</i>	Keck II/NIRSPEC Sep. 1999
								7200	<i>K</i>	VLT1/ISAAC Sep. 1999
								10 800	<i>H</i>	VLT1/ISAAC Nov. 1999
Q0256-000 C17	02 58 59.8	+00 10 52	...	3.280	23.89	0.82	...	10 800	<i>K</i>	VLT1/ISAAC Nov. 1999
Q0347-383 C5	03 49 43.5	-38 10 05	3.244	3.236	23.82	0.65	...	18 000	<i>K</i>	VLT1/ISAAC Nov. 1999
B2 0902+343 C12	09 05 43.8	+34 11 08	3.396	3.384	23.63	1.16	...	6300	<i>K</i>	Keck II/NIRSPEC Apr. 2000
								4500	<i>H</i>	Keck II/NIRSPEC Apr. 2000
West MMD11	14 18 09.7	+52 22 01	2.985	2.979	24.05	1.04	2.72	4500	<i>K</i>	Keck II/NIRSPEC Apr. 2000
Q1422+231 D78	14 24 40.5	+22 59 35	...	3.101	23.77	0.95	...	5400	<i>K</i>	Keck II/NIRSPEC Apr. 2000
Q1422+231 D81	14 24 31.4	+22 59 52	3.107	3.098	23.41	0.51	...	6300	<i>K</i>	Keck II/NIRSPEC Apr. 2000
								7200	<i>H</i>	Keck II/NIRSPEC Apr. 2000
3C324 C3	15 49 47.1	+21 27 05	3.295	3.283	24.14	0.85	0.75	2700	<i>K</i>	Keck II/NIRSPEC Apr. 2000
SSA22a MD46	22 17 27.3	+00 18 10	3.091	3.081	23.30	0.42	0.34	14 400	<i>K</i>	VLT1/ISAAC Sep. 1999
SSA22a D3	22 17 32.4	+00 11 33	3.086	3.075	23.37	0.97	0.40	7200	<i>K</i>	Keck II/NIRSPEC Sep. 1999
								5400	<i>H</i>	Keck II/NIRSPEC Sep. 1999
DSF 2237+116b C21	22 39 29.0	+11 50 58	3.410	3.394	23.47	0.86	...	10 800	<i>K</i>	VLT1/ISAAC Sep. 1999
DSF 2237+116a C2	22 40 08.3	+11 49 05	3.333	3.319	23.55	1.13	1.37	7200	<i>K</i>	Keck II/NIRSPEC Sep. 1999
Other objects:										
Q0000-263 D6 <sup>f</sup>	00 03 23.8	-26 02 49	2.971	2.961	22.88	0.45	0.42	21 600	<i>K</i>	UKIRT/CGS4 Sep. 1996
B2 0902+343 C6 <sup>f</sup>	09 05 20.5	+34 09 08	3.099	3.080:	24.13	0.45	1.21	21 600	<i>K</i>	UKIRT/CGS4 Nov. 1997
West CC13 <sup>g</sup>	14 18 02.5	+52 24 36	3.412	3.400	23.64	1.06	0.60	2700	<i>K</i>	Keck II/NIRSPEC Jun. 1999
MS 1512-cB58 <sup>h</sup>	15 14 22.3	+36 36 26	2.7326	2.7242	24.10	0.74	0.80	1800	<i>K</i>	Keck II/NIRSPEC Jun. 1999
								1800	<i>H</i>	Keck II/NIRSPEC Jun. 1999
								1200	<i>N4</i> <sup>i</sup>	Keck II/NIRSPEC Jun. 1999

<sup>a</sup> J2000 coordinates.

<sup>b</sup> Vacuum heliocentric redshift of Lyman  $\alpha$  emission when present.

<sup>c</sup> Vacuum heliocentric redshift of interstellar absorption lines. When less than three lines could be measured, the redshift is indicated as uncertain by a colon.

<sup>d</sup> Magnitudes are in the AB system; typical error is  $\pm 0.1$  mag.

<sup>e</sup> Magnitudes are in the AB system;  $K_{\text{AB}} = K_s + 1.82$ , where  $K_s$  is the magnitude on the Vega scale. Typical error is  $\pm 0.2 - 0.3$  mag.

<sup>f</sup> Pettini et al. 1998.

<sup>g</sup> Teplitz et al. 2000a.

<sup>h</sup> Teplitz et al. 2000b. The magnitudes (from Ellingson et al. 1996) have been corrected for the gravitational magnification by a factor of 30 derived by Seitz et al. 1998.

<sup>i</sup> NIRSPEC N4-band spans the wavelength range 1.3-1.6  $\mu\text{m}$ .

TABLE 2  
FLUXES AND STAR FORMATION RATES<sup>a</sup>

Name	$z_{\text{H II}}^b$	$\mathcal{R}$	$(G - \mathcal{R})_{\text{corr}}^c$	$L_{1500}^d$	$F_{\text{H}\beta}^e$	$W_{\text{H}\beta}^f$	$L_{\text{H}\beta}^g$	$\text{SFR}_{\text{H}\beta}^h$	$\text{SFR}_{\text{UV}}^i$
CDFa C8	3.0752	23.72	0.62	2.2	$1.1 \pm 0.2$	19	0.92	20	30
CDFa C1	3.1147	23.53	0.32	2.9	$3.4 \pm 1$	28	2.9	63	40
Q0201+113 C6	3.0548	23.92	0.29	2.0	$1.0 \pm 0.4$	19	0.78	17	27
Q0256–000 C17	3.2796	23.89	0.27	2.3	$\leq 0.45$	$\leq 8$	$\leq 0.43$	$\leq 9$	32
Q0347–383 C5	3.2337	23.82	0.15	2.0	$\leq 1.7$	$\leq 27$	$\leq 1.6$	$\leq 34$	28
B2 0902+343 C12	3.3866	23.63	0.49	3.0	$2.7 \pm 0.3$	37	2.8	61	42
West MMD11	2.9816	24.05	0.80	1.5	$1.2 \pm 0.3$	5	0.92	20	21
Q1422+231 D81	3.1037	23.41	0.15	3.2	$4.1 \pm 0.4$	43	3.4	74	45
SSA22a MD46	3.0855	23.30	0.07	3.2	$\leq 2.3$	$\leq 31$	$\leq 1.9$	$\leq 41$	44
SSA22a D3	3.0687	23.37	0.64	2.7	$1.3 \pm 0.3$	25	1.1	24	38
DSF 2237+116a C2	3.3176	23.55	0.54	3.1	$3.5 \pm 0.4$	25	3.5	75	44
Other objects:									
B2 0902+343 C6	3.091	24.13	0.18	1.7	$3 \pm 1$	40	2.5	54	24
West CC13	3.4062	23.64	0.38	3.0	$\leq 1.4^j$	$\leq 22$	$\leq 1.5$	$\leq 32$	42
MS 1512-cB58 <sup>k</sup>	2.7290	24.10	0.72	1.1	$1.35 \pm 0.2$	26	0.83	18	16

<sup>a</sup> $H_0 = 70 \text{ km s}^{-1} \text{ Mpc}^{-1}$ ,  $\Omega_{\text{M}} = 0.3$ ,  $\Omega_{\Lambda} = 0.7$ .

<sup>b</sup>Vacuum heliocentric redshift of nebular emission lines.

<sup>c</sup> $(G - \mathcal{R})$  colour corrected for Ly $\alpha$  forest opacity.

<sup>d</sup>Continuum luminosity at 1500 Å in units of  $10^{29} \text{ ergs s}^{-1} \text{ Hz}^{-1}$ .

<sup>e</sup>Line flux in units of  $10^{-17} \text{ ergs s}^{-1} \text{ cm}^{-2}$ .

<sup>f</sup>Rest-frame line equivalent width in Å.

<sup>g</sup>Line luminosity in units of  $10^{42} \text{ ergs s}^{-1}$ .

<sup>h</sup>Star formation rate ( $M_{\odot} \text{ yr}^{-1}$ ) deduced from the H $\beta$  luminosity (see text).

<sup>i</sup>Star formation rate ( $M_{\odot} \text{ yr}^{-1}$ ) deduced from the continuum luminosity at 1500 Å (see text).

<sup>j</sup> $3\sigma$  limit.

<sup>k</sup>Corrected for the gravitational magnification by a factor of 30 derived by Seitz et al. 1998.

TABLE 3  
LINE FLUXES AND THE ABUNDANCE OF OXYGEN

Name	$z_{\text{H II}}^a$	$K_{\text{AB}}^b$	$M_{\text{B}}^c$	$F_{\text{H}\beta}^d$	$F_{5007}^d$	$F_{4959}^d$	$F_{3727}^d$	$\log R_{23}^e$	$12+\log(\text{O}/\text{H})_{10}^f$	$12+\log(\text{O}/\text{H})_{\text{up}}^g$
Q0201+113 C6	3.0548	23.35	-22.20	$1.0 \pm 0.4$	$4.0 \pm 0.4$	$1.6 \pm 0.3$	$1.8 \pm 0.3$	0.66–1.03	7.62–8.37	8.32–8.78
B2 0902+343 C12	3.3866	(22.89)	(-22.84)	$2.7 \pm 0.3$	$7.4 \pm 0.3$	$3.4 \pm 0.3$	$3.9 \pm 1.3$	0.66–0.79	7.62–7.94	8.63–8.78
Q1422+231 D81	3.1037	(22.67)	(-22.91)	$4.1 \pm 0.4$	$18 \pm 1$	$7.5 \pm 0.5$	$4.0 \pm 0.7$	0.80–0.91	7.75–8.02	8.55–8.69
SSA22a D3	3.0687	22.97	-22.59	$1.3 \pm 0.3$	$8.5 \pm 0.4$	$1.9 \pm 0.5^h$	$3.2 \pm 0.6$	0.90–1.09	8.04–8.50	8.23–8.55
Other objects:										
MS 1512-cB58 <sup>i</sup>	2.7290	23.30	-22.04	$1.35 \pm 0.2$	$4.9 \pm 0.25$	$1.3 \pm 0.4$	$4.25 \pm 0.4$	0.82–0.95	8.01–8.29	8.39–8.59

<sup>a</sup>Vacuum heliocentric redshift of nebular emission lines.

<sup>b</sup> $K_{\text{AB}} = K_s + 1.82$ , where  $K_s$  is the magnitude on the Vega scale. Values in brackets have been calculated from the  $\mathcal{R}$  magnitudes listed in Table 1, assuming the mean color  $(\mathcal{R} - K_{\text{AB}}) = 0.74$ .

<sup>c</sup>Absolute magnitude in the rest-frame  $B$ -band, assuming  $H_0 = 70 \text{ km s}^{-1} \text{ Mpc}^{-1}$ ;  $\Omega_{\text{M}} = 0.3$ ;  $\Omega_{\Lambda} = 0.7$ .

<sup>d</sup>Line flux in units of  $10^{-17} \text{ ergs s}^{-1} \text{ cm}^{-2}$ .

<sup>e</sup> $R_{23} = ([\text{O II}] + [\text{O III}])/\text{H}\beta$ .

<sup>f</sup>Oxygen abundance deduced from the lower branch of the  $R_{23}$  relation.

<sup>g</sup>Oxygen abundance deduced from the upper branch of the  $R_{23}$  relation.

<sup>h</sup>This value is somewhat uncertain because the line is in a deep telluric absorption trough.

<sup>i</sup>Corrected for the gravitational magnification by a factor of 30 derived by Seitz et al. (1998).

TABLE 4  
KINEMATICS OF LYMAN BREAK GALAXIES

Name	$z_{\text{H II}}^a$	$K_{\text{AB}}^b$	$M_{\text{B}}^c$	$\Delta v_{\text{IS abs}} (\text{km s}^{-1})^d$	$\Delta v_{\text{Ly}\alpha} (\text{km s}^{-1})^e$	$\sigma (\text{km s}^{-1})^f$
CDFa D18	3.1122	(23.00)	(−22.58)	−420 :	+580 :	79 ± 7
CDFa C8	3.0752	23.19	−22.37	−300	...	106 ± 6
CDFa C1	3.1147	22.42	−23.17	−270	...	≤ 63
Q0201+113 C6	3.0548	23.35	−22.20	−130	...	64 ± 4
Q0256−000 C17	3.2796	(23.15)	(−22.53)	+60	...	53 ± 4
Q0347−383 C5	3.2337	(23.08)	(−22.58)	+140	+730	69 ± 4
B2 0902+343 C12	3.3866	(22.89)	(−22.84)	−170	+640	87 ± 12
West MMD11	2.9816	21.33	−24.18	−170	+230	53 ± 5
Q1422+231 D81	3.1037	(22.67)	(−22.91)	−420	+260	116 ± 8
3C324 C3	3.2876	23.39	−22.29	−340	+530	76 ± 18
SSA22a MD46	3.0855	22.96	−22.61	−340	+380	67 ± 6
SSA22a D3	3.0687	22.97	−22.59	+460	+1280	113 ± 7
DSF 2237+116a C2	3.3176	22.18	−23.52	+100	+1070	100 ± 4
Other objects:						
Q0000−263 D6	2.966	22.46	−23.04	−440	+380	60 ± 10
B2 0902+343 C6	3.091	22.92	−22.65	−800 :	+580	55 ± 15
West CC13	3.4062	23.04	−22.70	−420	+370	...
MS 1512-cB58	2.7290	23.30 <sup>g</sup>	−22.04 <sup>g</sup>	−390	+290	81

<sup>a</sup>Vacuum heliocentric redshift of nebular emission lines.

<sup>b</sup> $K_{\text{AB}} = K_s + 1.82$ , where  $K_s$  is the magnitude on the Vega scale. Values in brackets have been calculated from the  $\mathcal{R}$  magnitudes listed in Table 1, assuming the mean color  $(\mathcal{R} - K_{\text{AB}}) = 0.74$ .

<sup>c</sup>Absolute magnitude in the rest-frame  $B$ -band, assuming  $H_0 = 70 \text{ km s}^{-1} \text{ Mpc}^{-1}$ ;  $\Omega_{\text{M}} = 0.3$ ;  $\Omega_{\Lambda} = 0.7$ .

<sup>d</sup>Velocity offset of interstellar absorption lines relative to nebular emission lines. Values of  $z_{\text{abs}}$  are given in column 5 of Table 1.

<sup>e</sup>Velocity offset of  $\text{Ly}\alpha$  emission line relative to nebular emission lines. Values of  $z_{\text{Ly}\alpha}$  are given in column 4 of Table 1.

<sup>f</sup>One-dimensional velocity dispersion of nebular emission lines.

<sup>g</sup>Corrected for gravitational magnification by a factor of 30.

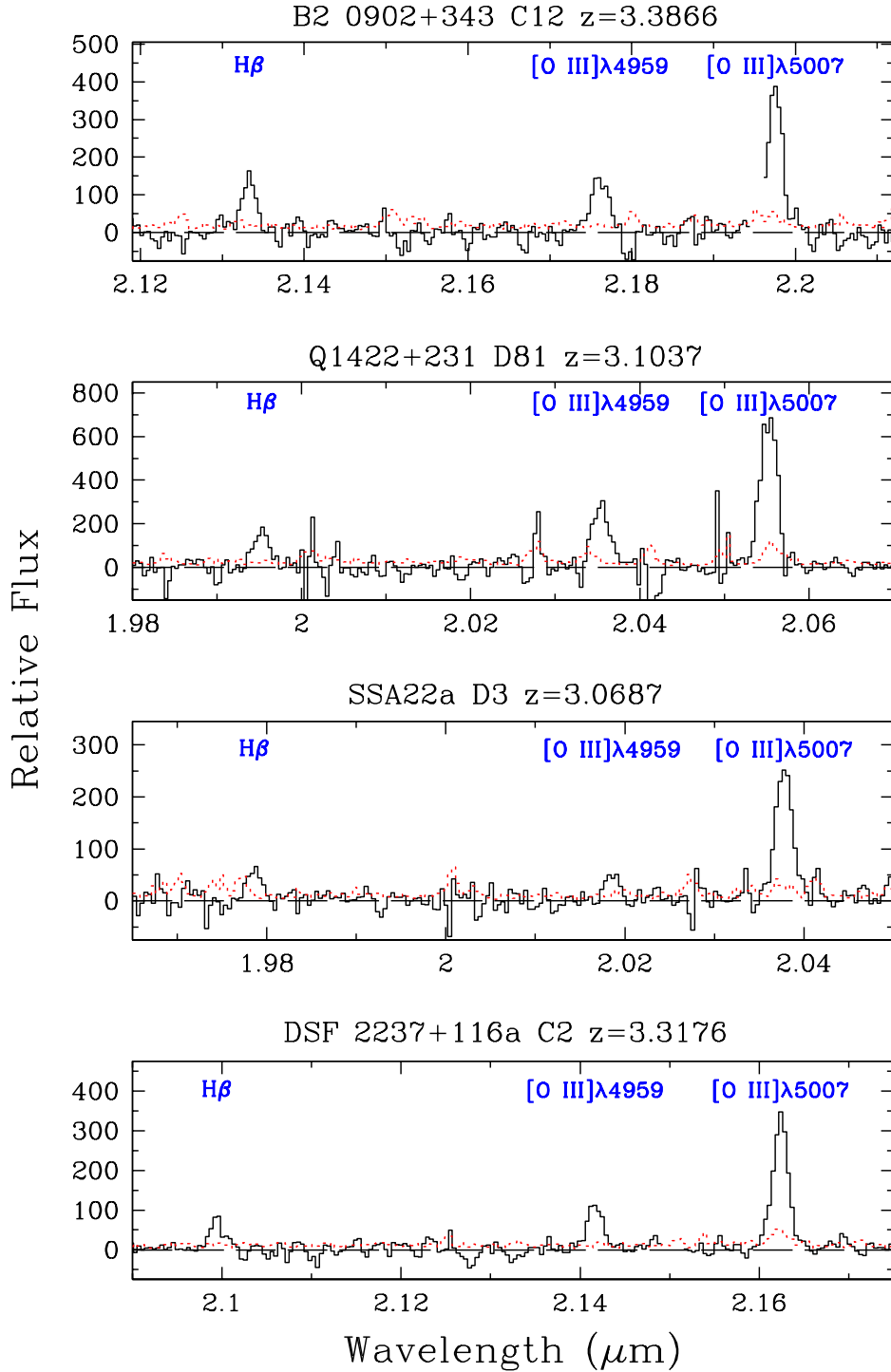


Fig. 1.— Examples of NIRSPEC  $K$ -band spectra of Lyman break galaxies. The resolving power is  $R \simeq 1500 - 1750$  sampled with three wavelength bins; the exposure time was typically  $\sim 2$  hours (see Table 1). In each panel the dotted line shows the  $1\sigma$  error spectrum. Gaps in the spectra correspond to invalid data points resulting mostly from poorly subtracted sky lines.



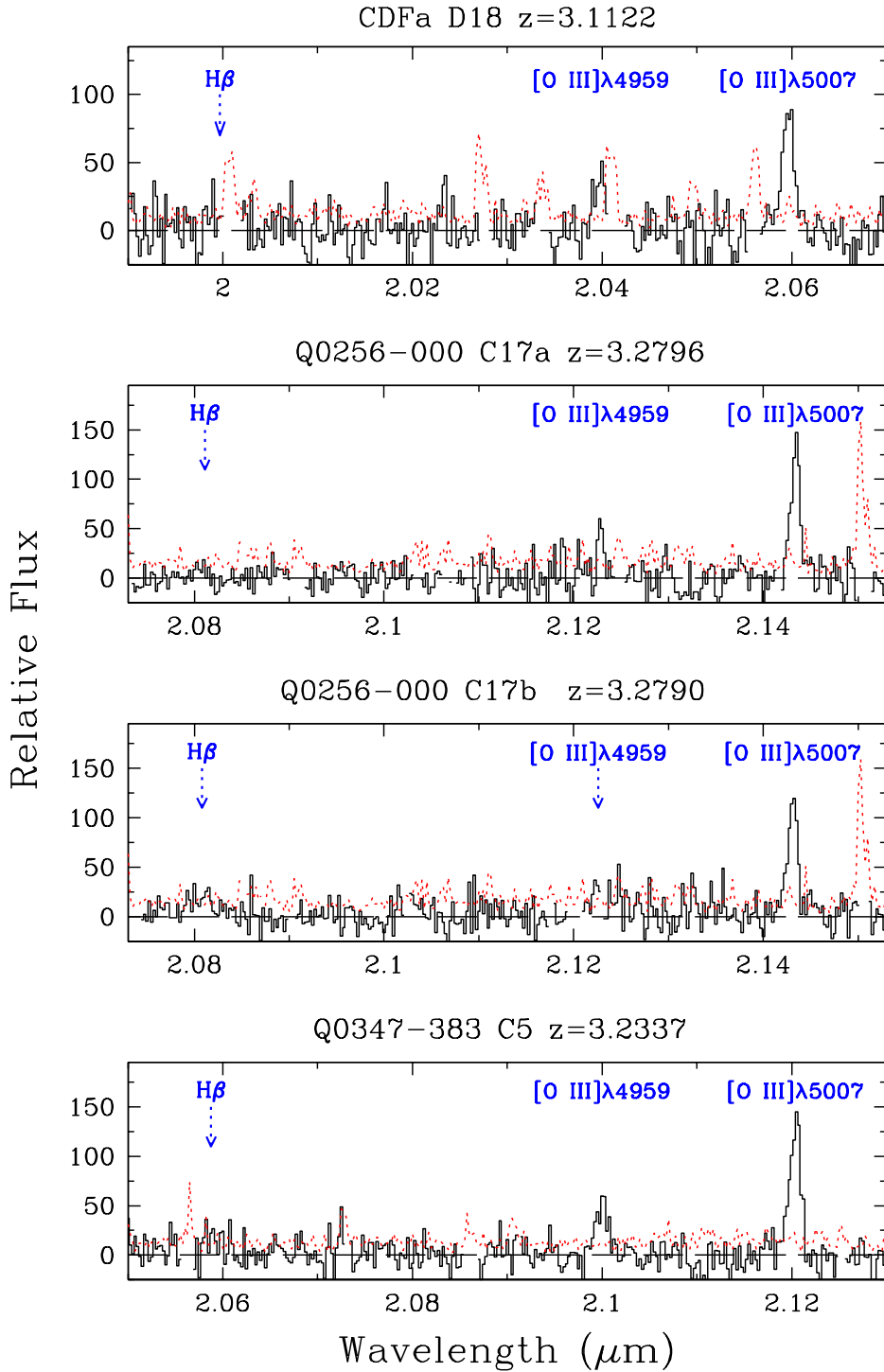


Fig. 2.— Examples of ISAAC  $K$ -band spectra of Lyman break galaxies. The resolving power is  $R \simeq 2750$ , sampled in this plot with three wavelength bins (each bin is twice the original pixel size). The exposure times were three hours, except for Q0347-383 C5 for which the exposure time was five hours. In each panel the dotted line shows the  $1\sigma$  error spectrum; the expected positions of *undetected* emission lines are indicated by downward pointing arrows.

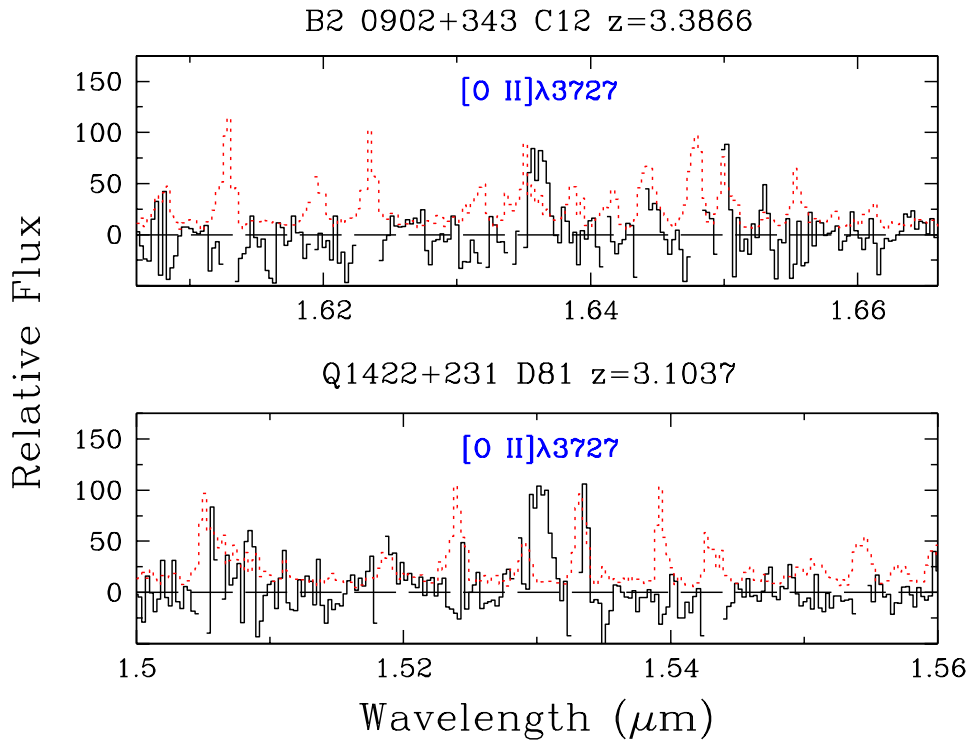


Fig. 3.— Examples of NIRSPEC  $H$ -band spectra of Lyman break galaxies. In each panel the dotted line shows the  $1\sigma$  error spectrum.

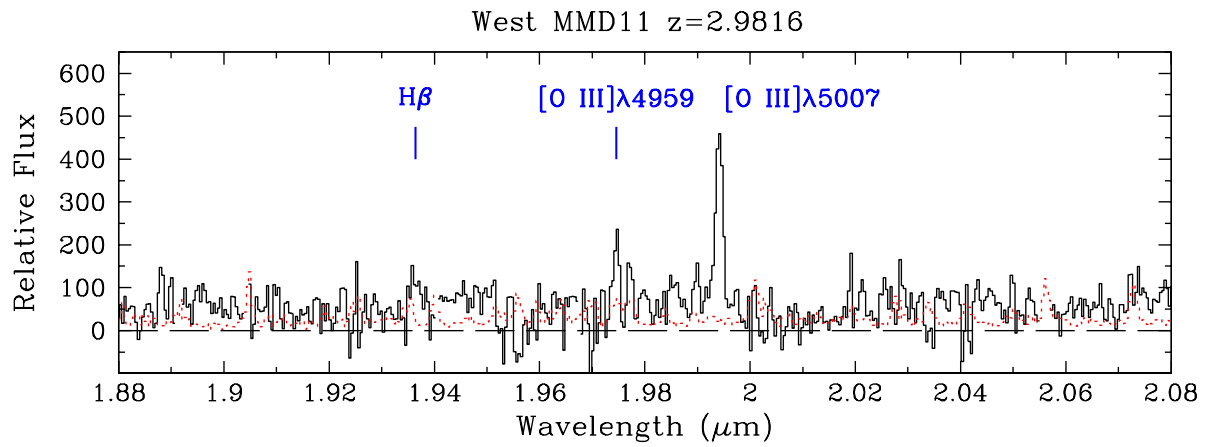


Fig. 4.— NIRSPEC  $K$ -band spectrum of West MMD11, one of the two Lyman break galaxies where we detect a clear continuum signal. The dotted line shows the  $1\sigma$  error spectrum.

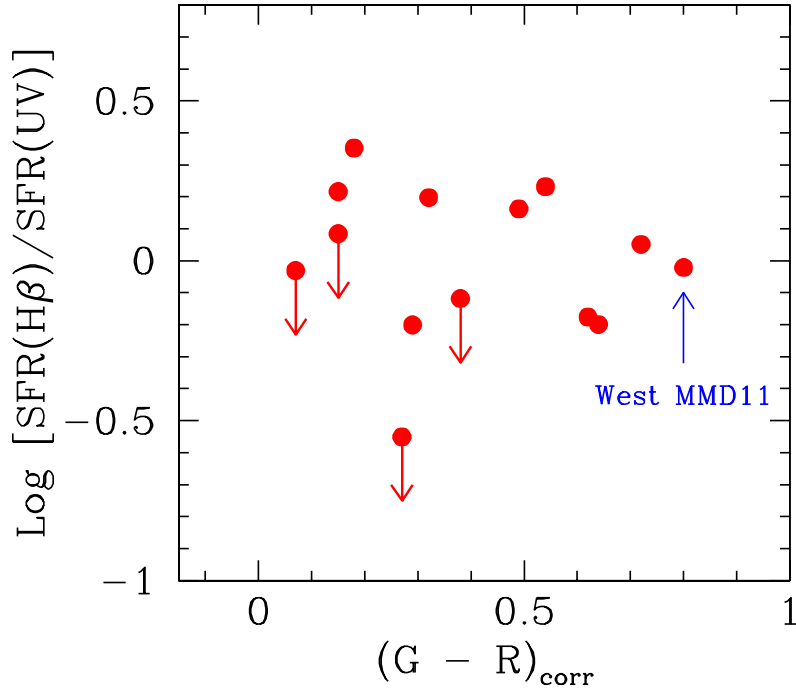


Fig. 5.— Comparison between the values of star formation rate deduced from the luminosities in the  $H\beta$  emission line and in the UV continuum at  $1500 \text{ \AA}$ . The color  $(G - \mathcal{R})$  measures the intrinsic UV spectral slope after statistical correction for the Lyman  $\alpha$  forest opacity. Note that in the SCUBA source West MMD11, which is also the reddest object in the present sample, the strength of  $H\beta$  relative to the UV continuum is typical of the rest of the sample and  $\text{SFR}_{H\beta} \simeq \text{SFR}_{UV}$ .

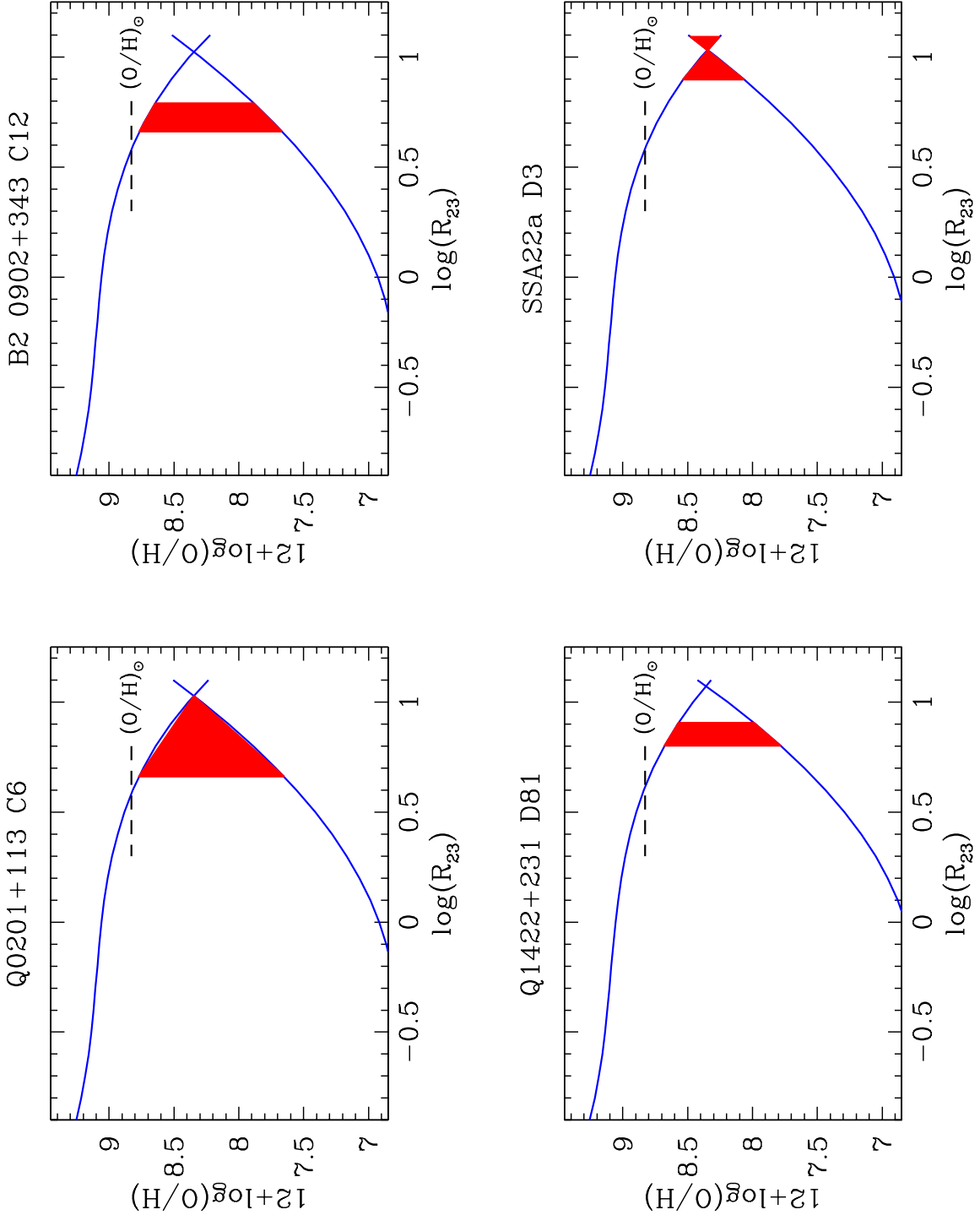


Fig. 6.— Oxygen abundance from the  $R_{23} = ([\text{O II}] + [\text{O III}])/\text{H}\beta$  ratio. In each panel the continuous lines are the calibration by McGaugh (1991) for the ionization index  $O_{32} = [\text{O III}]/[\text{O II}]$  appropriate to that object. The shaded area shows the values allowed by the measured  $R_{23}$  and its statistical  $1\sigma$  error. The broken horizontal line gives for reference the most recent estimate of the solar abundance  $12 + \log(\text{O}/\text{H}) = 8.83$  (Grevesse & Sauval 1998).

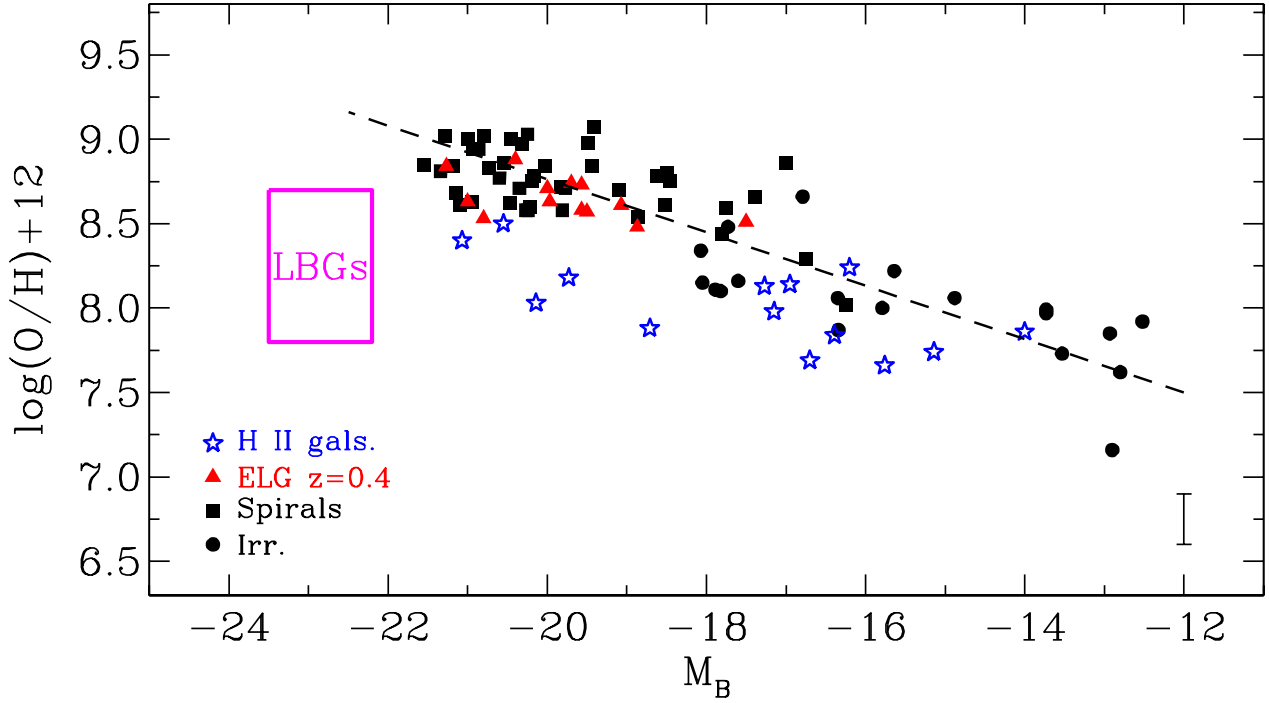


Fig. 7.— Metallicity-luminosity relation for local galaxies, from the compilation by Kobulnicky & Koo (2000) adjusted to the  $H_0 = 70 \text{ km s}^{-1} \text{ Mpc}^{-1}$ ,  $\Omega_M = 0.3$ ,  $\Omega_\Lambda = 0.7$  cosmology adopted in this paper. The vertical bar in the bottom right-hand corner gives an indication of the typical error in  $\log(\text{O}/\text{H})$ . In the Sun  $12 + \log(\text{O}/\text{H}) = 8.83$  (Grevesse & Sauval 1998). The box shows the approximate location of the Lyman break galaxies in our sample at a median  $z = 3.1$ . Like many local H II galaxies, LBGs are overluminous for their metallicity. The height of the box results largely from the double-valued nature of the calibration of  $(\text{O}/\text{H})$  in terms of the  $R_{23}$  index (see Figure 6); the one case where the ambiguity can be resolved (MS 1512-cB58) lies in the upper half of the box.

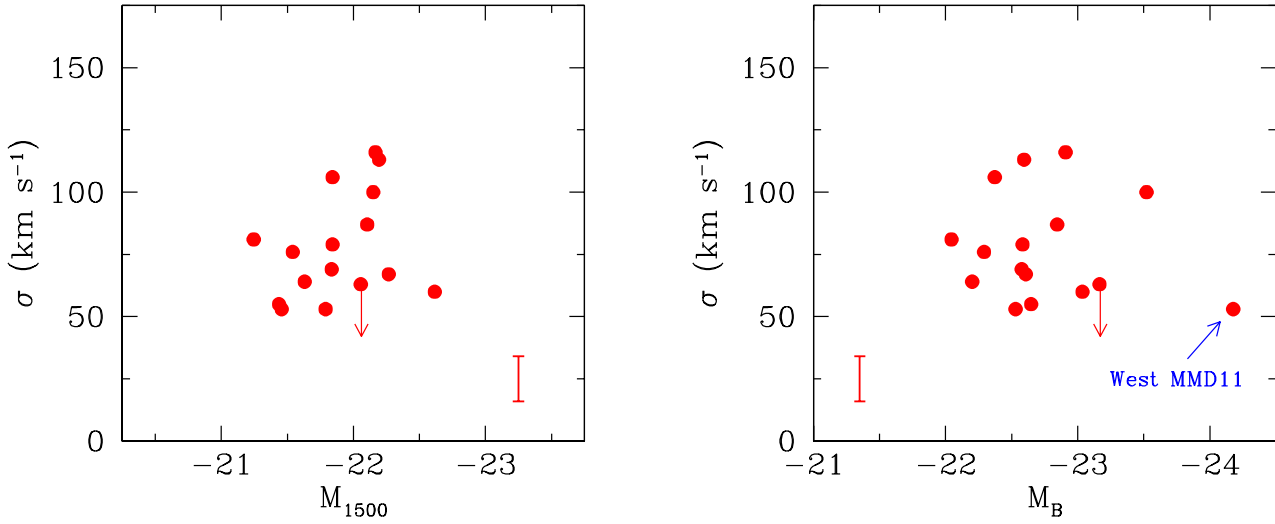


Fig. 8.— One dimensional velocity dispersion of nebular emission lines in Lyman break galaxies as a function of absolute magnitude in the rest-frame far-UV (left) and  $B$ -band (right). The vertical bar shows the typical error on the measurements of  $\sigma$ . Curiously, the SCUBA source West MMD11, which has the reddest ( $\mathcal{R} - K$ ) color in the present sample, exhibits one of the smallest velocity dispersions.

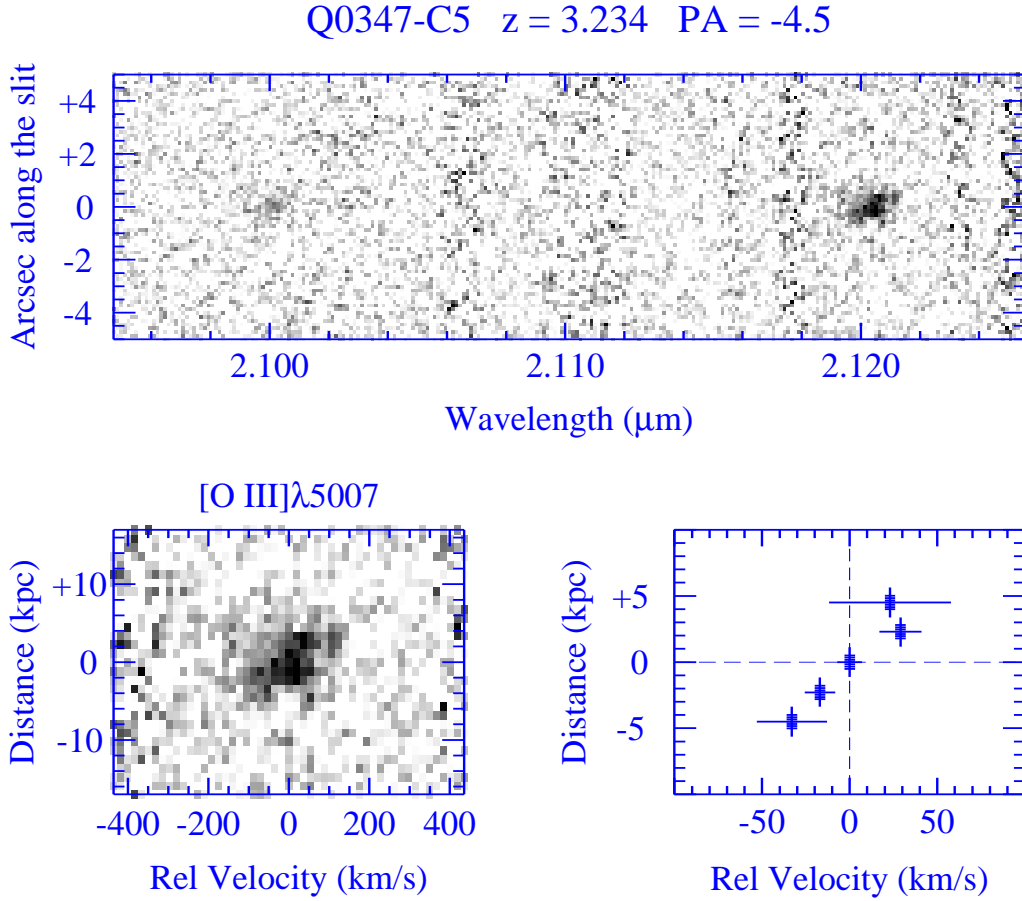


Fig. 9.— Spatially resolved emission in ISAAC spectra. The top panel shows (on a negative scale, so that black is bright) a portion of the final, stacked 2-D image encompassing the [O III]  $\lambda\lambda 4959, 5007$  doublet obtained with a total integration time of 18 000 s. The bottom left-hand panel is an enlargement of the  $\lambda 5007$  line; the projected linear scale is for our adopted  $H_0 = 70 \text{ km s}^{-1} \text{ Mpc}^{-1}$ ,  $\Omega_M = 0.3$ ,  $\Omega_\Lambda = 0.7$ , cosmology. The bottom right-hand panel shows how the central wavelength of the emission line varies along the slit. The spatial resolution of the image is 0.62 arcsec FWHM (4.7 kpc).



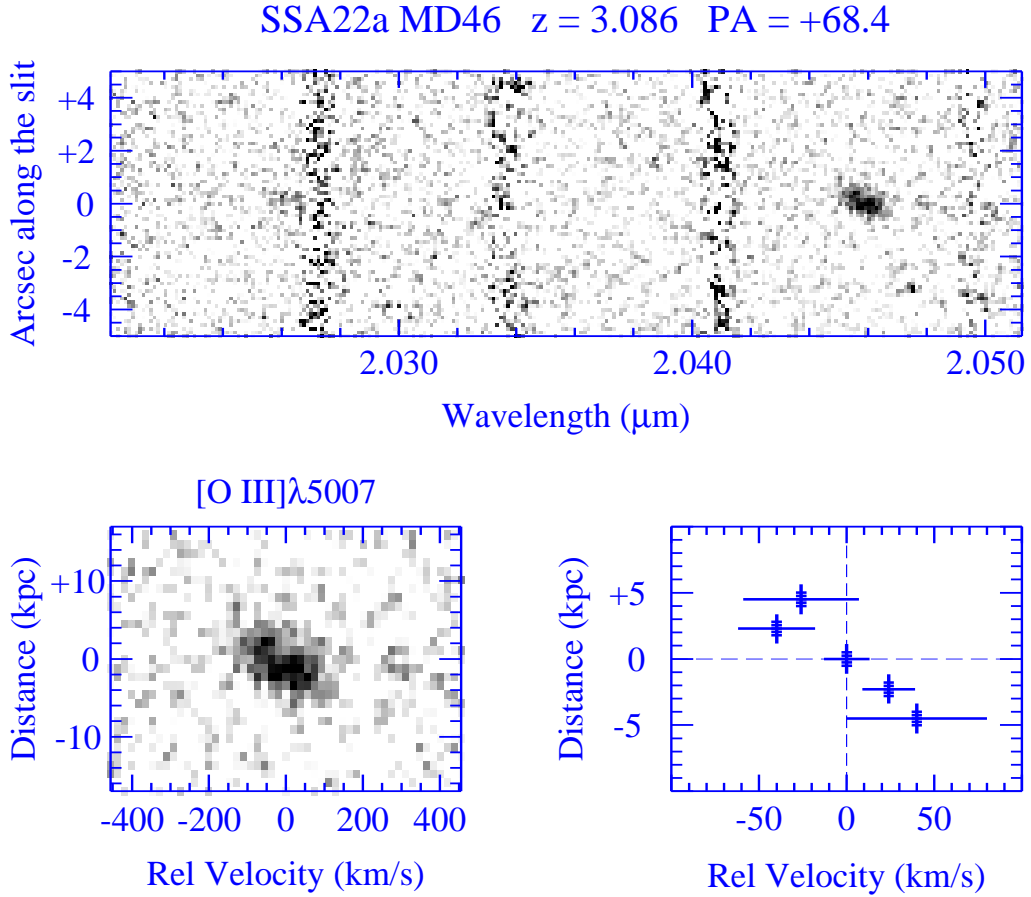


Fig. 10.— Spatially resolved emission in ISAAC spectra. The top panel shows a portion of the final, stacked 2-D image encompassing the [O III]  $\lambda\lambda$ 4959, 5007 doublet obtained with an integration time of 14 400 s. The vertical bands are residuals left from the subtraction of strong OH sky lines. The bottom left-hand panel is an enlargement of the  $\lambda$ 5007 line; the bottom right-hand panel shows how the central wavelength of the emission line varies along the slit. The spatial resolution of the image is 0.64 arcsec FWHM (4.9 kpc).

Q0347-383 C5  $z = 3.2337$

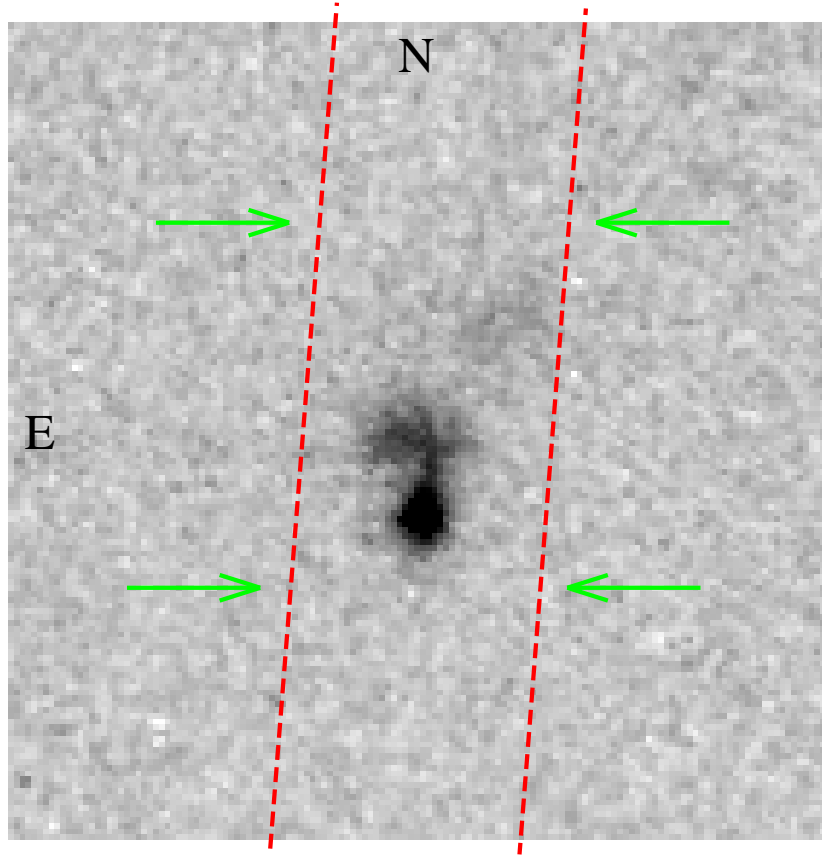


Fig. 11.— WFC2 image of Q0347–383 C5 obtained through the F702W filter with a total exposure time of 18 000 s. The dashed lines indicate the edges of the 1 arcsec wide ISAAC slit. The horizontal arrows mark the limits of the [O III]  $\lambda 5007$  emission shown in Figure 9, recorded in 0.62 arcsec seeing.

SSA22a MD46  $z = 3.0855$

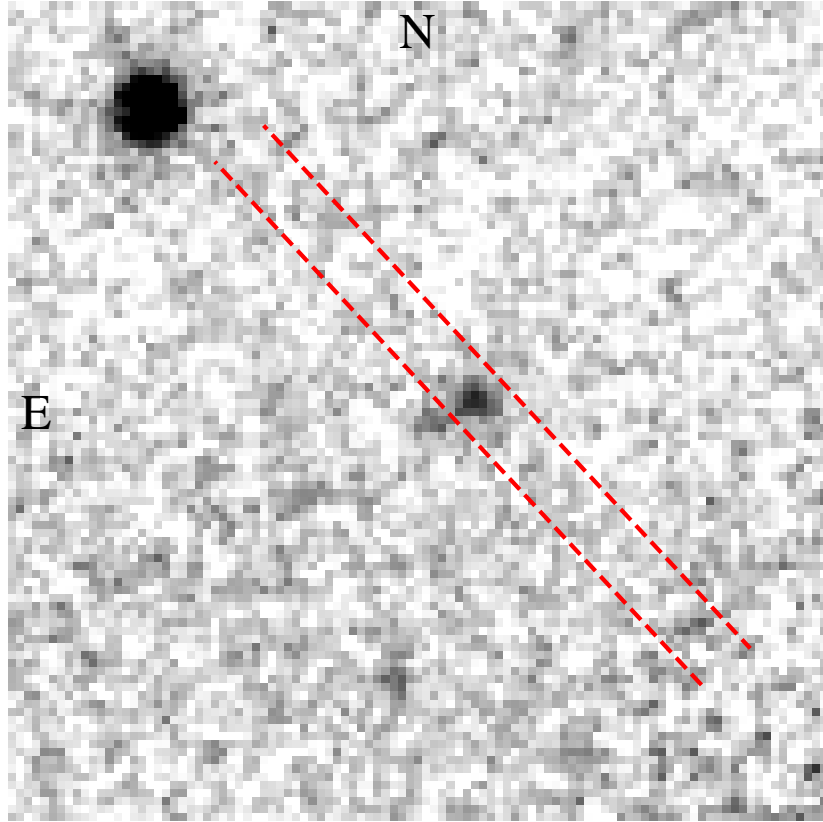


Fig. 12.—  $K$ -band image of SSA22a MD46 obtained with NIRC in  $\sim 0.5$  arcsec seeing. The total integration time was 3240 s made up of six sets of exposures, each consisting of  $9 \times 60$  s frames recorded in a nine-point dither pattern. The 1 arcsec wide ISAAC slit is overlaid.

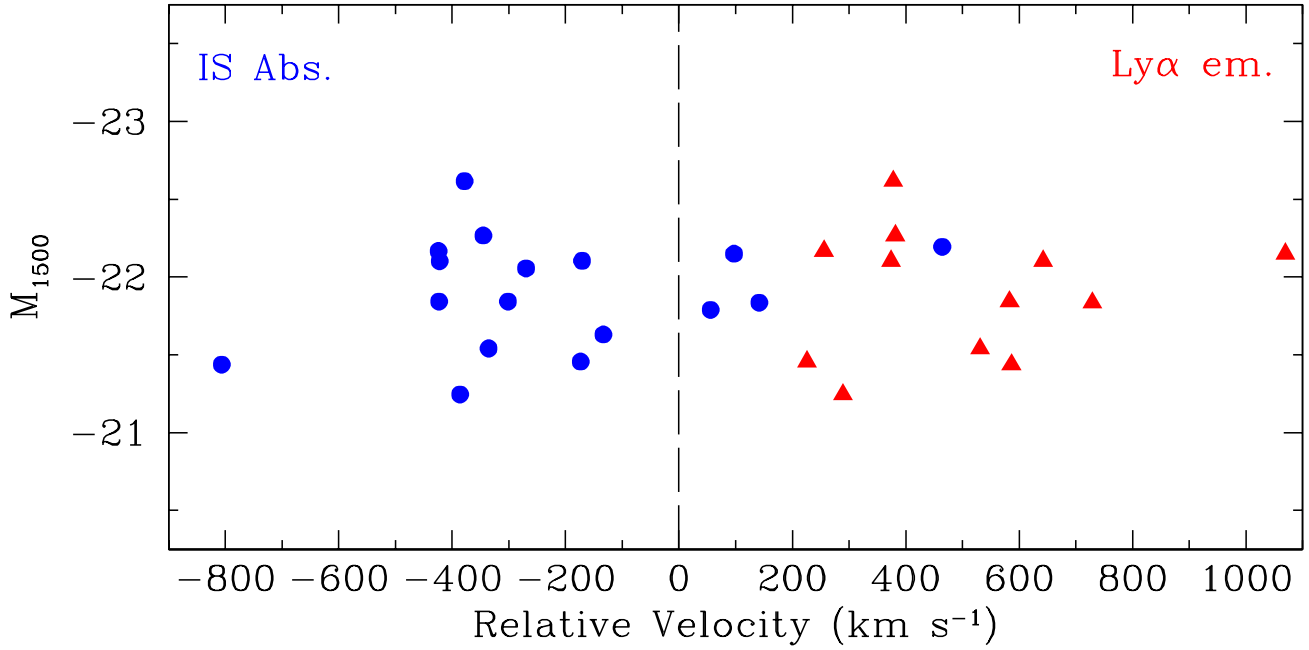


Fig. 13.— Velocity offsets in Lyman break galaxies. The dots and the triangles correspond respectively to the values of  $\Delta v_{\text{IS abs}}$  and  $\Delta v_{\text{Ly}\alpha}$  listed in Table 4 and indicate the velocity differences, relative to [O III] and  $\text{H}\beta$ , of the interstellar absorption lines and of the Lyman  $\alpha$  emission line. Large scale motions of the order of several hundred  $\text{km s}^{-1}$  are indicated by the systematic tendency for the former to be blueshifted and the latter redshifted relative to the nebular emission lines. Plotting these measurements as a function of  $M_{\text{B}}$  shows a very similar picture—we find no correlation between values of  $\Delta v$  and absolute magnitude in either the far-UV or the optical.